Arterial vascular patterning: a crosstalk between angiogenic and shear stress signaling.

Dongying Chen[1,*], Oleksii S. Rukhlenko[2], Divyesh Joshi[1], Martina Rudnicki[7], Brian G. Coon[1,#], Raja Chakraborty[1], Anna Tuliakova[2], Elena Ioannou[7], Kathleen A. Martin[1], Boris N. Kholodenko[2,3,4,], Christiana Ruhrberg[7], Martin A. Schwartz[1,5,6,*], Michael Simons[1,5,*]

[1] Yale Cardiovascular Research Center, Department of Internal Medicine, Yale University School of Medicine, New Haven, United States.
[2] Systems Biology Ireland, School of Medicine, University College Dublin, Dublin, Ireland.
[3] Conway Institute of Biomolecular & Biomedical Research, University College Dublin, Dublin, Ireland
[4] Department of Pharmacology, Yale University School of Medicine, New Haven, United States.
[5] Department of Cell Biology, Yale University School of Medicine, New Haven, CT, United States.
[6] Department of Biomedical Engineering, Yale University, New Haven, CT, United States.
[7] UCL Institute of Ophthalmology, London, UK
[#] Current address: Cardiovascular Biology Research Program, Oklahoma Medical Research Foundation, Oklahoma City, United States
* Corresponding authors:
Dongying Chen: dongying.chen@yale.edu
Martin A. Schwartz: martin.schwartz@yale.edu
Michael Simons: michael.simons@yale.edu

Abstract

Morphogenesis of the postnatal developing vasculature involves two essential processes: angiogenesis, which is responsible for the formation and expansion of the capillary bed, and arteriogenesis, which remodels a part of the capillary bed into the arterial vasculature. A rich pool of studies over the past two decades suggested that the vascular endothelial growth factor A (VEGF-A, VEGF hereafter unless otherwise specified), the primary inducer of angiogenesis, also promotes arteriogenesis. However, this fails to explain the spatiotemporal segregation of angiogenesis and arteriogenesis during postnatal vascular morphogenesis. It is also unclear how the same molecule, a proliferation-inducing growth factor, can be responsible for two very different processes, one of which (angiogenesis) requires active cell proliferation and the other (arteriogenesis) requires growth arrest. Interestingly, arterial specification in VEGF loss-of-function (LOF) animal models has not been examined. Here, we report that physiological doses of VEGF do not induce arterial fate in capillary endothelial cells, instead serving as a physiological brake to slow down fluid shear stress (FSS)-driven capillary-to-arterial fate transition. Studies in four different mouse models with fully or partially disrupted VEGF signaling show impaired angiogenesis but preservation of arteriogenesis, accompanied by ectopic arterialization particularly in the artery-associated capillary bed. The interplay of VEGF and FSS, two essential environmental cues guiding vascular morphogenesis, converges on the mechanosensitive transcription factor Sox17 that regulates expression of key arterial fate genes. We conclude that while angiogenic signaling promotes vascular expansion and protects the capillary bed from premature and ectopic arterialization driven by blood flow, cessation of angiogenic signaling is required to permit FSS-driven arteriogenesis. These findings establish a new paradigm of VEGF-FSS crosstalk coordinating angiogenesis, arteriogenesis and capillary maintenance during vascular morphogenesis.

Vasculature in the brain and retina forms by several complementary processes: expansion of the capillary bed by vessel sprouting, venous differentiation and remodeling of the capillary bed into arteries in a process termed arteriogenesis[1-3]. The vascular endothelial growth factor VEGF-A (VEGF hereafter) is a key driver of vascular growth in both the brain and retina[2-6].VEGF's role as a driver of spouting angiogenesis has been clearly established, including its role in inducing filopodia-studded endothelial tip cells that lead new vessel sprouts[6,7], and its cross talk with DLL4-driven notch signaling[8,9]. VEGF and Notch signaling, including their cross talk, has also been implicated in promoting arteriogenesis[10-13]. For example, studies of dorsal aorta formation in zebrafish and mouse showed that VEGF induces Dll4, and that Notch activation is essential for arterial specification[10,13,14]. Moreover, it has been suggested that angiogenesis and arteriogenesis are functionally linked via Notch signaling[15,16]. Overexpression of the Notch intracellular domain (NICD), which constitutively activates notch signaling, also increases arterialization[17]. Vice versa, endothelial-specific knockout of Dll4 or treatment with a gamma secretase inhibitor DAPT that inactivates Notch signaling, causes vascular hypersprouting whilst also decreasing arterial morphogenesis[8,10,11,15,16,18-20]. Collectively, these findings led to a model in which VEGF, the primary stimulus for angiogenesis, also regulates arterial fate specification, potentially by modulating Notch signaling.

However, this paradigm does not explain the spatiotemporal separation of angiogenesis and arteriogenesis in a developing vasculature, as arterialization does not take place at the angiogenic front where VEGF levels are the highest. Also, it has not been resolved how VEGF, an endothelial growth factor capable of stimulating cell proliferation can also promote arterial fate specification, considering that the latter process requires cell cycle arrest[21]. Moreover, the model of VEGF-induced Notch signaling coupling angiogenesis and arteriogenesis has not yet been integrated with current knowledge of fluid shear stress (FSS)-induced Notch signaling, which regulates arterial specification and maintains arterial homeostasis[21,22]. Furthermore, the relative importance of VEGF and FSS in arterial fate specification has not previously been determined. If both are drivers of arteriogenesis, the combination of the two inputs would have an additive effect on arterialization in the capillary region. Finally, despite many studies focused on angiogenesis in VEGF loss-of-function (LOF) mouse lines, arteriogenesis in these mice has never been examined.

To address these problems, we set out to examine interactions of VEGF and FSS on induction of arterial specification in capillary endothelial cells in vitro and in the developing mouse retina. We report here that VEGF signaling serves as a critical physiological brake to attenuate FSS-driven arterial fate acquisition. Not only does VEGF not promote arterial fate, FSS-driven capillary-to-artery cell fate transition requires cessation of VEGF signaling. Mechanistically, VEGF antagonizes the FSS-activated arterial program by decreasing the transcription activity of Sox17 on arterial promoters and enhancers. Based on these findings, we propose a novel paradigm by which VEGF-FSS competition coordinates angiogenesis, arteriogenesis and capillary maintenance. This new concept fully addresses the issues mentioned above, thereby resolving the long-standing controversies in vascular morphogenesis and paving a new avenue for clinical considerations on therapeutic vascularization.

Results

VEGF counteracts FSS-induced capillary-to-artery endothelial cell fate transition.

To test the roles of VEGF and FSS in arterial fate specification during capillary bed remodeling, we used human microvascular blood endothelial cells (HMVBECs, primary capillary endothelial cells) to examine the induction of arterial genes under four experimental conditions: static flow (ST), VEGF in static flow (VEGF), laminar flow (FSS), and a combination of laminar flow and VEGF (FSS+VEGF)(Fig.1a-c). Analysis of the RNAseq transcriptomic data clustered the arterial and capillary genes separately and revealed a pattern of gene expression inversely regulated by VEGF and FSS

(Fig.1a). FSS, but not VEGF, effectively induced the arterial profile, including definitive arterial genes Gja4, Gja5, Sox17, Efnb2, Sema3g, Cxcl12, Nrp1 and Jag1, and inhibited the capillary profile (Emcn, Flt4 and Mfsd2a) (Fig.1a). In contrast, VEGF decreased the FSS-induced arterial profile and maintained the capillary profile inhibited by FSS (Fig.1a-c). RNA and protein expression patterns of these genes expression were validated by RT-PCR and western blotting (Fig.1b-c), except that expression of capillary genes Tfrc and Ivns1abp did not show statistically significant results (Fig.1b-c). These results indicate that FSS promotes capillary-to-artery cell fate transition, while VEGF counteracts this process to maintain the capillary fate (Fig.1a, diagram).

To further validate these results obtained in HMVBECs, we used human umbilical venous endothelial cells (HUVECs) to examine arterial induction in the same experimental setting (Fig.S1). The expression patterns of most definitive arterial genes (Gja4, Gja5, Sema3g, Efnb2, Jag1) in HUVECs in response to VEGF, FSS and FSS+VEGF were highly consistent with the results in HMVBECs (Fig.S1). There were two exceptions: Sox17 (more induction in FSS+VEGF than FSS) and Nrp1 (no significant induction by VEGF, FSS or FSS+VEGF)(Fig.S1), likely due to the venous and embryonic nature of HUVECs.

To further test the VEGF/FSS interaction on arterial specification, we used HMVBECs to examine the induction of arterial genes in various VEGF and FSS gradients. We find that VEGF inhibited the FSS-induced arterial program in a dose-dependent manner (Fig.1d). Among the arterial genes examined, Gja5 and Gja4 were the most sensitive to VEGF inhibition, as the lowest dose (2ng/ml) of VEGF was sufficient to completely compromise the FSS-driven induction of these genes (Fig.1d). Moreover, induction of arterial genes by FSS gradient (0, 5, 12, 18, 24 dyn/cm^2) were effectively suppressed by VEGF(Fig.1e).

To better understand the capillary-to-artery cell state transitions, we applied a systems biology approach termed cell the State Transition Assessment and Regulation (cSTAR) analysis[23-25] to further analyze our transcriptomic data (Fig.1f, detailed description in the legend). cSTAR analysis showed that the four experimental conditions (ST, VEGF, FSS, FSS+VEGF) resulted in four different metastable EC states (Fig.1f). The combination of FSS+VEGF led to a new EC state distinct from the FSS state or the VEGF state, which is not a reversion process that VEGF brings the FSS state to the baseline state (ST). This suggests that there are distinct programs activated by VEGF and FSS, respectively, with little overlap between the two.

Collectively, these findings demonstrate that, during arterial specification, the transition from capillary fate to arterial fate is governed by the VEGF/FSS crosstalk: FSS promotes capillary-to-artery transition and VEGF counteracts this process to maintain capillary fate.

Arteriogenesis takes place in the capillary regions with reduced VEGF activity.

The data presented above prompted us to re-examine the spatiotemporal relationship between angiogenesis and arteriogenesis as well as the relationship between VEGF, FSS, and arterial morphogenesis. In the mouse postnatal retina, vascular morphogenesis begins at a postnatal day 0(P0)-1 when nascent vessels begin to sprout from the central vein[7,26], with a rudimentary capillary plexus emerging by P2 (Fig.2a). At P2-3, when a capillary bed is formed, arteries appeared in the central part of the capillary plexus, as identified by high-level expression of the arterial marker Sox17 (Sox17^{high}), (Fig.2a). At P3-4, while sprouting activity continues to lead the angiogenic front, arteriovenous patterning transforms the capillary bed into a hierarchical vascular structure with capillaries, arteries and veins (Fig.2a). By P4-5, the whole vasculature developed into a stereotypical vascular tree: the arteries and the veins aligned in an alternating pattern in the central area, the angiogenic sprouts at the periphery driving vascular expansion towards the avascular zone, and the capillary bed in the middle. (Fig.2a). Of note, although both angiogenesis and arteriogenesis progress from the retinal center to the periphery (Fig.2a, retinal periphery at the top and retinal center at the bottom), arteriogenesis lags behind as demonstrated by the un-arterialized gaps between the Sox17^{high}-labeled arterial tip and the angiogenic

front (Fig.2a). Therefore, angiogenesis and arteriogenesis are spatiotemporally segregated during vascular morphogenesis.

In this developing vasculature, EdU incorporation and endothelial phospho-ERK (pERK) signal identified endothelial cells with presumably high level of VEGF activity, predominantly at the angiogenic front at the periphery of the P5 retina (Fig.2b). The extent of both endothelial pERK and EdU-labeled proliferation declined in the capillary region undergoing arterialization and almost completely disappeared in arterioles and arteries (Fig.2b), consistent with the previous report[27]. By contrast, FSS was present in the entire developing vasculature, as visualized by retro-orbital injection of isolectin B4 (IB4-iv), except for unlumenized angiogenic sprouts at the vascular front (Fig.2b). These observations demonstrate that arterial morphogenesis takes place in the portion of the capillary bed where FSS is present while VEGF activity has decreased and that there is no association between high VEGF activity and arteriogenesis.

Intriguingly, the spatial segregation of angiogenesis and arteriogenesis creates an un-arterialized artery-associated capillary zone between the arterial tip and angiogenic front (Fig.2c). We refer to this region here as the "*Arterial Delta*" (AΔ), where arterial blood vasculature extends and branches throughout the capillary network in a manner resembling a river delta (Fig.2c). This region is exposed to both high levels of VEGF and post-arterial levels of FSS, but without arterialization (Fig.2b-c).

VEGF signaling is not required for arterial specification during capillary remodeling.

Our observation that arteriogenesis occurs in the capillary region where VEGF activity has declined raises the question whether VEGF is in fact required for arterial fate specification. Despite ample studies of angiogenesis, arteriogenesis in VEGF loss-of-function (LOF) mice has never been formally examined. Therefore, we used a comprehensive set of VEGF LOF mouse strains to examine the role of VEGF in arteriogenesis. Given that artery formation is a result of capillary remodeling, we defined arterial extension as the ratio of the Sox17^{high} blood vessel (the artery) to the radial outgrowth of the capillary bed labeled by IB4, expressed as a percentage, with 100% representing full extension to the vascular margin. As a reciprocal analysis, the un-arterialized gap from the Sox17^{high} arterial tip to the vascular front was measured and expressed as the percentage of the un-arterialized distance in the radial outgrowth. In addition, mural smooth muscle coverage of the forming artery was examined by SMA antibody staining.

First, we evaluated the effect of the inducible global deletion of VEGF, the principal activator of VEGFR2, using Cag-CreER^{TM} driver to globally delete the *Vegfa* gene (hereafter *Vegfa*^{iKO}), as retinal VEGF is mostly produced in the neural bed[4]. Tamoxifen injection to activate the Cre driver was started at P2 when the initial capillary bed is formed with minimal arteriogenesis. As expected, such an early deletion of VEGF led to a significant reduction in vascular outgrowth and capillary density (Fig.3a). Nevertheless, immunostaining with anti-Sox17 and -SMA antibodies revealed the presence of arteries displaying high level of Sox17 expression (Sox17^{high}), and the mural smooth muscle coverage, both in control and *Vegfa*^{iKO} retinas (Fig.3a). Arterial extension in the control retina was 80.3%±4.8% (mean±SD) with an un-arterialized gap of 19.7%±4.4% (Fig.1a). At the same time, in the *Vegfa*^{iKO} retinas, Sox17^{high}-labeled arterial extension was significantly increased (95.1%±5.1%), with ectopic arterialization in the vascular front (indicated by arrow heads) and a strikingly reduced size of the un-arterialized gap (4.9%±5.1%) (Fig.3a). Of note, 83.3%±14.2% of all individual arteries measured in the *Vegfa*^{iKO} retinas reached 100% extension with no un-arterialized gap, a phenotype of increased arterialization not found in the control retinas (Fig.1a). Arterial smooth muscle coverage exhibited high level of variability in the *Vegfa*^{iKO} retinas, with a mildly reduced mean (47.3%±22.8%), compared to 59.5%±9.5% in the control retinas. (Fig.3a). These observations suggest that, despite mild impaired mural smooth muscle coverage, arterial specification in the endothelium remains intact upon global VEGF deletion.

Next, we examined the effect of an inducible endothelial deletion of VEGFR2 using Cdh5CreER^{T2} driver (hereafter *Vegfr2*^{iECKO}) with tamoxifen injection similarly initiated at P2 (Fig.3b). Though mean

Sox17^{high}-labeled arterial extension in the *Vegf2*^{iECKO} retinas (84.2%±10.7%) was comparable to the control (79.2%±3.3%), arterial phenotype demonstrated high level of variability (Fig.3b). Individual measurements per artery revealed that 28.6% of the Sox17^{high}-labeled arteries reached 100% (full) extension in the *VEGFR2*^{iECKO} retinas, with ectopic arterialization at the vascular front, which was not observed in the control retinas (Fig.3b). Mural muscularization also exhibited high variability in the *VEGFR2*^{iECKO} retinas, with an average (48.1%±14.6%) mildly reduced compared with the control (58.1%±3.6%) (Fig.3b). In addition, ectopic muscularization was detected at the vascular front and veins in some *Vegfr2*^{iECKO} retinas. Overall, arterial specification is intact in the *VEGFR2*^{iECKO} retinas, in line with the phenotype in the *Vegfa*^{iKO}.

To exclude the possibility that intact arterial specification is due to incomplete gene deletion, we evaluated the effectiveness of VEGFR2 deletion in the *VEGFR2*^{iECKO} retinas by immunostaining with anti-VEGFR2 antibody (Fig.3c). In the control retina, VEGR2 signal was present in blood vessels as well as in the neural bed (Fig.3c), consistent with a previous report[4]. Intriguingly, in the *VEGFR2*^{iECKO} retina, VEGFR2 staining was absent in the blood vessels but remained present in the neural bed, creating an appearance of “empty grooves” in a VEGFR2+ background (Fig.3c). These results confirm nearly complete and specific deletion of endothelial VEGFR2 in the *VEGFR2*^{iECKO} retina. Notably, VEGFR2^{null}/Sox17^{high} ECs highlighted the artery-like vessels (Fig.3c), direct evidence of arterial fate specification independent of VEGFR2.

Taken together, these observations suggest that VEGF/VEGFR2 signaling is not required for the acquisition of arterial fate by the capillary endothelium.

Blocking VEGF signaling leads to ectopic arterialization in the Arterial Delta.

Although arterial specification remains intact in the *Vegfa*^{iKO} and *VEGFR2*^{iECKO}retinas, severe vascular rarefaction in these mice may directly and indirectly affect global and local hemodynamic force, endothelial and mural cell physiology and subsequent arterial maturation. Also, global loss of VEGF in the *Vegfa*^{iKO} retinas potentially impaired pericytic VEGF-VEGFR1 signaling[28,29]. To address these issues, we used alternative approaches to block endothelial VEGF signaling without deleting the ligand and receptor, thereby leaving VEGF and VEGFR2 intact and available for other biological activities.

First, we tested DC101, a well-studied neutralizing antibody that specifically blocks the binding of murine cognate ligand VEGF to its receptor VEGFR2[30,31]. DC101 was injected intra-peritoneally into neonatal mice at P1 and P3 and the retinas were analyzed as described above. DC101 treatment significantly impaired vascular growth and density, confirming effective blockade of VEGFR2 signaling, while substantially preserving the capillary bed (Fig.4a). Notably, immunostaining of Sox17 and SMA revealed extensive arterialization in the developing vasculature (Fig.4a). All arteries in the DC101-treated retina spanned from the retinal center to the vascular front, reaching 100% arterial extension, with complete disappearance of the un-arterialized gap (Fig.4a). Ectopic arterialization, marked by both Sox17^{high} and SMA signals, was found in the Arterial Delta region of capillary extending further to the veins, leaving only the capillary between the main arteries and veins un-arterialized across the vasculature (Fig.4a).

Next, we tested the effect of endothelial-specific deletion of *Plcg1*. Although PLCγ1 mediates multiple signaling pathways, it is the primary docking effector of VEGFR2 signaling and plays only subordinate roles in other growth factors signaling[32,33]. Endothelial deletion of PLCγ1 (hereafter *Plcg1*^{iECKO}) at P1-3 significantly impaired angiogenesis at P6, but with better preservation of the vascular bed(Fig.4b) compared with the *Vegfa*^{iKO} and *VEGFR2*^{iECKO} retinas (Fig.3). Arterial extension was remarkably increased in the *Plcg1*^{iECKO} retinas, with 52.7% of Sox17^{high}-labeled arteries reaching 100% extension (Fig.4b). Ectopic arterialization marked by both Sox17^{high} and SMA signals was evidenced in the Arterial Delta region of capillary in the *Plcg1*^{iECKO} retinas (Fig.4b). Though to a less extent, these

arterial phenotypes are in line with the DC101-treated retinas, indicating increased arterial specification with mature mural muscularization.

Due to the lack of workable staining antibody, deletion of endothelial PLCγ1 in P6 pups were analyzed using isolated brain ECs in order to acquire enough cells for qPCR analysis. The results demonstrate 70% reduction of *plcg1* mRNA as detected by the primers targeting exons2-3 and comparable levels of *plcg1* mRNA by the primers targeting exons 24-26, which confirms effective gene deletion of plcg1 despite the presence of a truncated plcg1 mRNA (Fig.S2).

In summary, DC101 treatment and endothelial deletion of PLCγ1 effectively block VEGFR2 signaling, which leads to intact arterial formation and ectopic arterialization the Arterial Delta region.

Fluid shear stress (FSS)-induced arterial specification is independent of VEGFR2 signaling.

Since the arterial specification program is intact in the VEGF LOF animal models, we set out to investigate whether FSS is capable of driving arterial fate in the absence of VEGF signaling. FSS requires the presence of blood flow and, hence, vascular lumenization. We conducted an in vivo staining by retro-orbitally injecting IB4-Alexa488 (IB4-iv) to visualize vascular patency and the presence of blood flow (Fig.5a). Dissected retinas were counterstained with IB4-Alexa647 to visualize the whole vasculature, including the patent and the closed vessels (Fig.5a). In control retinas, while the majority of vessels were double-stained, the absence of IB4-iv identified the un-lumenized sprouts at the vascular front and some regressed vessels around the arteries (Fig.5a), indicating a lack of blood flow in these vessels. Importantly, the DC101-treated, *Vegfr2*^{iECKO} and the *Plcg1*^{iECKO} vessels were well double-stained (Fig.2a), suggesting that there was effective blood flow through these vessels and that endothelial cells with defective VEGFR2 signaling were exposed to the hemodynamic force (FSS)..

With these in vivo data in hand, we next tested whether blocking VEGFR2 signaling affects FSS-induced arterial specification in HUVECs in vitro. HUVECs treated with siPLCγ1 were able to respond to arterial level of laminar FSS (12 dynes/cm^2) with effective induction of arterial genes, including Sox17, Gja4, Gja5, Efnb2 and Notch target Hey1(Fig.5b), indicating an intact FSS-induced arterial program upon blocked VEGF signaling.

Taken together, these in vivo and in vitro findings indicate that FSS-induced arterial specification is independent of VEGFR2 signaling, which well explains the phenotype of intact arterial specification in VEGF LOF mouse models.

Blocking VEGFR2 signaling promotes capillary-to-artery transition in the single cell transcriptome.

To gain mechanistic insights into VEGF LOF arterial phenotypes, we performed single-cell RNAseq analysis of endothelial cells (ECs) from control and *Plcg1*^{iECKO} mice retinas. Among 30 cell clusters identified in UMAP (uniform manifold approximation and projection) plots, 1505 cells in cluster 12 with endothelial identity (*Pecam1*+, *Cdh5*+*; Cldn5*+) were selected for further analysis (Fig.S4). Published markers of endothelial phenotypes (Table S1) were used to annotate endothelial zonation in the arterial-capillary-venous axis and determine cell cycle status based on gene expression profiles (Fig.S5). The following 10 EC subclusters were identified (0-9) (Fig.S5a and Fig.6a): a sprouting cluster (cluster 6, *Esm1*^{high}*;Kcne3*^{high}), an arterial cluster (cluster 9, *Gja4* ^{high}*; Gja5*^{high}*; Efnb2*^{high}*; Sema3g*^{high}*; Gkn3*^{high}*; Bmx*^{high}*; Sox17*^{high}*; Cxcl12*^{high}*; Unc5b*^{high}, most cells in G1 phase), capillary/venous clusters (clusters 0, 2, 3, 4 and 7, *Aplnr*^{high}*; Mfsd2a*^{high}*; Ivns1abp*^{high}*; Flt4*^{high}*; Tfrc* ^{high}*; slc38a5* ^{high}*; Nr2f2* ^{high}*; Nrp2* ^{high}*; Ephb4* ^{high}), an arterial predecessor cluster (cluster 8, with both arterial and capillary profiles) and a proliferative cluster (cluster 0, with capillary/venous profile, all cells in G2M/S phases) (Fig.S5b-f). In addition, the ECs in cluster 5 display weak endothelial identity with low expression of endothelial markers (Cdh5, Cldn5, Pecam1, Flt1, Kdr and Erg), likely ECs from regressing vessels (Fig.S5e). The identity of Cluster 1 is

281 unclear, as these ECs express low levels of capillary/venous markers and some endothelial markers
282 (Cdh5, Cldn5 and Kdr) (Fig.S5d-e).
283 In the *Plcg1*^{iECKO} transcriptome, the percentages of ECs in the proliferative cluster 0 and capillary
284 clusters 2, 3 and 7 were substantially reduced (Fig.6b), consistent with the phenotype of defective
285 angiogenesis in the *Plcg1*^{iECKO} retinas. Notably, the *Plcg1*^{iECKO} arterial predecessors in cluster 8 (purple
286 color) exhibited a substantial increase (19% in *Plcg1*^{iECKO} versus 3% in the control), with a pattern of
287 distribution spreading into and mixed with capillary clusters 4 and 7 (Fig.6b), suggesting increased
288 capillary-to-artery transition in the capillary of the *Plcg1*^{iECKO}.
289 To test this hypothesis, we performed a trajectory analysis to understand the dynamic transition of
290 differentiation states among EC clusters (Fig.6c-d). Pseudo-time analysis by TSCAN revealed a major
291 *capillary-to-artery (C-to-A)* differentiation trajectory starting from the proliferative cluster 0 to
292 capillary/venous clusters 4 and 7 and ending at the arterial predecessor cluster 8 and the arterial cluster
293 9 (Fig.6c). Besides this main trajectory, there were 3 side trajectories branching from the capillary clusters:
294 proliferative cluster 0 transitioned to cluster 5 with weak EC identity, likely a process of vascular
295 regression; capillary/venous cluster 4 transitioned to sprouting cluster 8; capillary/venous clusters 7
296 transitioned to clusters 3, 2, 1 (Fig.6c). Above all, trajectory analysis using RNA velocity revealed an
297 intact C-to-A differentiation trajectory in the *Plcg1*^{iECKO} transcriptomes (Fig.6d), thereby proving that the
298 increase of *Plcg1*^{iECKO} arterial predecessors in cluster 8 (Fig.6b) is a result of increased C-to-A transition.
299 In agreement with our in vitro and in vivo findings above (Fig.2-5), this scRNAseq analysis supports
300 the conclusion that blocking VEGFR2 signaling promotes C-to-A cell fate transition during capillary
301 remodeling.
302
303 **VEGF does not significantly alter FSS-induced cell cycle arrest.**
304 FSS-induced cell cycle arrest is a prerequisite for arterial specification[21]. Given the role of VEGF in
305 promoting proliferation, we tested whether it antagonizes the FSS-driven arterial program by altering cell
306 cycle arrest induced by the FSS. We first conducted transcriptomic analysis of the major cell cycle
307 regulators in the 4 experimental conditions mentioned above (ST, VEGF, FSS, FSS+VEGF, for 16 hours).
308 Differential gene expression clustering showed a clear demarcation between expression patterns of the
309 VEGF- and FSS-regulated cell cycle gene sets (Fig.S6a). FSS effectively silenced activators for G2/M-
310 phase (Cdk1, Ccnb1, Aurka, Aurkb), S-phase (Ccnd1, cdk4) and S/G2 (Ccna1, cdk2), while FSS
311 upregulated pan-cell cycle inhibitors (cdkn1a, cdkn1b) and G1/S activators (Ccne1, cdk6), demonstrating
312 a clear pattern of G1/S arrest (Fig.S6a). These gene sets were regulated by VEGF in a completely
313 opposite way (Fig.S6a). However, except for the downregulation of cdkn1b and cdk6, the overall gene
314 expression pattern of FSS+VEGF was not significantly different from the one of FSS (Fig.S6a). We
315 validated most of these cell cycle regulators using RT-PCR (Fig.S6b). Consistent with these results, EdU
316 incorporation assay confirmed that FSS effectively silenced proliferation, which was not significantly
317 changed in the condition of VEGF+FSS (Fig.S6c).
318
319 **Notch inhibition does not affect the VEGF-FSS crosstalk.**
320 Notch signaling is an important feature of the arterial vasculature. Since both VEGF and FSS are
321 inducers of Notch signaling, we sought to investigate whether it is involved in VEGF-FSS crosstalk to
322 regulate arterial specification. To this end, HMVBECs were pretreated with 5μM DAPT for 3h to eliminate
323 Notch activity, which was confirmed by the near absence of cleaved Notch intracellular domain (NICD)
324 (Fig.S6) and then subjected to the FSS, followed by analysis of the arterial fate gene expression. Notch
325 inhibition did not affect FSS-induced expression Sox17, Sema3G, and Jag1 that were induced in
326 comparable levels in DAPT treated cells as in controls, indicating that the induction is Notch-independent
327 (Fig.S6). At the same time, the induction of Efnb2, Gja5, Gja4 and Dll4 was partially or completely

328 compromised, indicating a requirement of Notch signaling (Fig.S6). Notably, VEGF attenuation of the
329 FSS arterial induction (Gja4, Gja5, Sox17, Sema3g, Efnb2 and Jag1) was not affected by DAPT treatment
330 (Fig.S6). Therefore, although Notch regulates expression of some of the arterial fate genes, Notch
331 signaling is not central to VEGF-FSS crosstalk-dependent regulation competition of arterial specification.
332
333 **Sox17 is a mechanosensitive transcription factor essential for the FSS-induced arterial program.**
334 The uniform response of the definitive arterial genes to the FSS-VEGF crosstalk suggests a common
335 transcription control point. To investigate this possibility, we used the bioinformatic tool TRANSFAC to
336 identify the presence of various transcription factors binding sites in arterial and capillary genes. This
337 analysis identified the presence of predicted binding motifs for the transcription factor Sox17 in proximal
338 promoters and/or the introns of all arterial and Notch genes, including Sox17 itself, but not in the capillary
339 genes (Table S3). By contrast, the predicted binding motifs for the Notch transcription regulator Rbpj
340 were not found in arterial genes Sox17 and Gja4 but were present in some capillary genes (Table S3).
341 These findings suggest that Sox17 is a unique transcription regulator of the arterial specification program.
342 Previous studies have shown that endothelial deletion of Sox17 impairs arteriogenesis in mouse
343 postnatal retina[17,34], but the role of Sox17 in FSS mechanotransduction signaling is unclear. To answer
344 this question, we performed Sox17 loss- and gain-of-function analysis. First, we used CRISPR cas9 to
345 knock out Sox17 in HUVECs to test its requirement for FSS to induce other definitive arterial genes. As
346 predicted, the loss of Sox17 profoundly compromised the FSS-induced arterial program, resulting in
347 almost no induction of Gja5, Gja4, Sema3g, Efnb2 and Nrp1 and a reduced induction of Unc5b and Jag1
348 (Fig.7a). By contrast, CRISPR cas9-mediated deletion of Sox18, another SoxF factor reported to have a
349 compensatory role to Sox17 in arteriogenesis in mouse retina[34], exhibited only modest effect on the FSS
350 induction of Gja4 and Efnb2 without affecting the induction of other arterial genes tested here (Fig.7a). A
351 combined knockout of Sox17 and Sox18 did not enhance the effect of Sox17 knockout alone on the FSS-
352 arterial program (Fig.7a). Therefore, Sox17, but not Sox18, is required to mediate the FSS-induced
353 arterial program.
354 Next, we tested whether high level of Sox17 can render the FSS irrelevant to the arterial program
355 induction. To this end, we used a lentivirus to create a doxycycline (Dox)-inducible Sox17 overexpression
356 system in HUVECs (Dox-Sox17-HUVECs). Dox-induced Sox17 overexpression effectively activated the
357 arterial program at static condition (Fig.7b). Importantly, there was a dose-dependent induction of
358 induction of Gja5, Gja4, Sema3g, Efnb2, Dll4 and Unc5b by Sox17 expression (Fig.7b).
359 Taken together, these findings identify Sox17 as a key mechanosensitive transcription factor for the
360 FSS-induced arterial program.
361
362 **VEGF antagonizes Sox17 transcription activity on arterial promoters and enhancers.**
363 Given the central role played by Sox17 in FSS-dependent arterial fate induction, we next examined
364 whether VEGF antagonizes the FSS program by suppressing Sox17 activity. To this end, we examined
365 the effect of VEGF treatment on arterial gene induction in the Dox-Sox17-HUVEC system discussed
366 above (Fig.7b). We found that, without lowering the expression level of Sox17, VEGF effectively inhibited
367 Sox17-activated transcription of the definitive arterial genes, including Gja5, Gja4, sema3g, Jag1, Cxcl12
368 and Efnb2 (Fig.8a). Moreover, the antagonizing effect of VEGF on Sox17-induced arterial program was
369 dose-dependent (Fig.8b), which completely recapitulates the dose-dependent effect of VEGF on
370 inhibiting the FSS-arterial program (Fig.1d). As a positive control, the induction of Unc5b and Dll4, two
371 known VEGF-Notch targets enriched in both arterial and sprouting ECs[8,35], was further enhanced by
372 VEGF (Fig.8a), proving a genuine effect of VEGF signaling in this experiment.
373 Since the antagonizing effect of VEGF does not rely on reducing Sox17 expression (Fig.8a-b, Fig.S1),
374 we tested whether it affects Sox17's transcriptional activity in arterial promoters and recently reported

375 arterial enhancers[36] using a chromatin immunoprecipitation (ChIP) assay to pull down Sox17-bound
376 chromatin in the Dox-Sox17-HUVEC system. The cells were either subjected to no treatment (NT), Dox
377 alone or a Dox+VEGF combination (Fig.8c). As expected, Dox-induced Sox17 expression led to
378 enrichment of Sox17 binding on arterial promoters and enhancers, including the proximal promoters of
379 Gja5, Gja4, Sema3g, Jag1, Cxcl12 and Efnb2, and arterial enhancers Gja5-7, Gja5-78, Gja4+50,
380 Cxcl12+269 (Fig.8c), confirming the role of Sox17 as a transcription regulator in the arterial program.
381 Critically, VEGF effectively inhibited the enrichment of Sox17 on these arterial promoters and enhancers
382 (Fig.8c), in line with the effect of VEGF on Sox17-induced expression of the arterial program (Fig.8a).
383 Taken together, these findings show that VEGF counteracts the FSS-induced arterial program by
384 compromising the transcription activity of Sox17 on arterial genes (Fig.8d).
385
386 **Discussion**
387 The data presented above identifies how VEGF/FSS crosstalk balances vascular growth and
388 patterning, during which angiogenic and arteriogenic signaling interact via the control of transcription
389 factor Sox17 as the key driver of capillary-to-arterial fate transition. FSS induces arterial fate gene
390 expression in microvascular endothelial cells, and this induction is counteracted by VEGF. Therefore, the
391 condition with high VEGF and low FSS favors angiogenesis, while the one with low VEGF and high FSS
392 favors arteriogenesis (Fig.9a).
393 Several lines of evidence support these conclusions. In vitro, FSS induced arterial gene expression
394 in HMVBECs and HUVECs, while VEGF inhibited this induction in a dose-dependent manner. In vivo,
395 developing retinal vasculature shows a clear spatiotemporal segregation of angiogenesis (early, on the
396 periphery, in the area of high VEGF levels) and arteriogenesis (late, central, in the areas of low VEGF
397 levels). Suppression of the VEGF/VEGFR2 signaling achieved either genetically (VEGF, VEGFR2, and
398 PLCγ1 knockouts) or with a VEGF neutralizing antibody (DC101) resulted in preserved arteriogenesis
399 with ectopic arterialization, while angiogenesis was impaired (Fig.9b). These data confirm that VEGF is
400 required for forming and expanding the capillary bed[37-39], but the process of FSS-driven capillary
401 remodeling into arterial vasculature is independent of VEGFR2 signaling. Furthermore, VEGF serves as
402 a physiological brake to counteract FSS-driven arteriogenesis, thus maintaining the capillary bed and
403 preventing ectopic arterialization, while a reduction in VEGF-VEGFR2 signaling input is required for the
404 FSS-driven arteriogenesis (Fig.9b).
405 This paradigm explains why there is a lack of arterialization in the artery-associated capillary region
406 (Arterial Delta) exposed to both VEGF and post-arterial level of FSS (Fig.9b). Most importantly, this
407 territory where VEGF-FSS crosstalk takes place, demonstrates a spatiotemporal segregation of vascular
408 growth and patterning (angiogenesis at the periphery, arteriogenesis in the central region) that is
409 essential for building a fully developed vasculature. Blocking VEGF signaling removes the physiological
410 brake for arteriogenesis in the Arterial Delta territory, thereby inducing ectopic arterialization. This leads
411 to the loss of capillary bed, compromising tissue oxygen and nutrient delivery, removal of metabolic waste
412 products, exchange of water and solutes and other functions of the normal microvasculature (Fig.9b, right
413 panel). On the other hand, physiological decrease in VEGF signaling in the central region allows for
414 effective FSS-driven arterial patterning leading to the development of new arterial vasculature. Finally,
415 our in vivo and in vitro data clearly indicates that VEGF signaling is not required for arterial specification
416 during capillary remodeling, which is governed by FSS as the genuine driver.
417 Previous studies have suggested that VEGF induction of Dll4 expression and the subsequent
418 activation of Notch signaling is the key to arteriogenesis[10,12,13]. However, Notch signaling functions as
419 negative feedback to downregulate VEGF signaling[8,18,20] and arrest cell cycle progression[21], thereby
420 serving as switch to terminate angiogenesis and allow activation of FSS-driven arteriogenesis. This
421 mechanistic control well known for tip-stalk conversion makes VEGF signaling transient at the

422 dynamically moving vascular front. Although constitutively active Notch signaling can induce arterial
423 specification[17,21], transient VEGF signaling at physiological doses is likely insufficient to create a
424 persistent Notch signaling to induce arterial fate. Moreover, it has also been proposed that the tip cells
425 that competitively acquire high VEGF-Notch signaling are selectively committed to arterial fate as "pre-
426 arterial" ECs at the vascular front[16,40]. Our scRNAseq transcriptomic analysis of wild type P6 retinal
427 vasculature shows that the cluster of sprouting ECs does not have a distinct "pre-arterial" expression
428 profile of any definitive arterial genes (e.g. Gja4, Gja5 and Sema3g) (Fig.S4). Finally, despite its partial
429 involvement in the FSS-arterial program, our data indicates that Notch signaling is not central to the
430 VEGF-FSS crosstalk.

431 In this study, we analyzed arterial morphogenesis in a comprehensive set of VEGF LOF mice. While
432 each intervention led to distinct phenotypes, in all cases there was a reduction in angiogenesis whereas
433 arteriogenesis was maintained or even increased. In addition, ectopic arterialization was found in the
434 Arterial Delta region of capillaries, leading to the disappearance of the un-arterialized gap. DC101
435 treatment in particular led to extensive ectopic arterialization in this territory. This likely reflects better
436 preservation of the capillary bed, thereby allowing more widespread capillary-to-artery fate transitions
437 facilitated by the blockade of VEGFR2 signaling that leaves the FSS-driven arteriogenesis program
438 unopposed. Furthermore, while DC101 specifically blocks VEGF-dependent activation of VEGFR2
439 signaling, it does not block ligand-independent functions of VEGFR2 such as mechanosensing and other
440 biological activities driven by its numerous co-receptors and partner proteins such as VEGFR1, integrins,
441 Nrp1, and Sdc2 among others[41-49]. Therefore, while *VEGFR2*^{iECKO} potentially jeopardizes other essential
442 signaling pathways besides intracellular signaling, DC101 treatment leaves non-tyrosine kinase signaling
443 functions of VEGFR2 intact. Furthermore, severe vascular rarefaction in *Vegfa*^{iKO}, *Plcg1*^{iECKO} and
444 *VEGFR2*^{iECKO} mice likely impairs normal heart development and/or function, reducing cardiac output and
445 resulting in decreased FSS. Severe vascular rarefaction in these mice also potentially created uneven
446 blood flow in the regressing capillary region, further weakening the magnitude of the FSS. By contrast,
447 the preservation of a substantial capillary bed in the DC101-treated retinas, likely due to incomplete
448 neutralization of VEGFR2 activation as indicated by the modest loss of the capillary bed, provides a more
449 permissive vascular environment with effective level of the FSS. These findings also illustrate the need
450 for effective angiogenesis-arteriogenesis coupling[50] and the need for formation of the adequate capillary
451 bed to support effective arteriogenesis.

452 While the arterial vasculature in *Vegfa*^{iKO} and *Plcg1*^{iECKO} mice retinas show similar magnitudes of
453 Sox17^{high}-labeled arterial extension, there are distinct differences in the extent of smooth muscle
454 coverage in *Vegfa*^{iKO} compared to *Plcg1*^{iECKO} mice. This difference likely reflects a more profound
455 inhibition of VEGFR2 signaling in the absence of VEGF (*Vegfa*^{iKO}) than PLCγ1 deletion and thereby a
456 difference in the preservation of the capillary bed for arteriogenesis. Indeed, although PLCγ1 knockout
457 blocks the signaling from VEGFR2-Y1173, signaling from other tyrosine phosphorylation sites of
458 VEGFR2, such as Y951, Y1054, Y1059, Y1214, is retained. Furthermore, the uncoupling of arterial
459 specification from mural smooth muscle coverage in the *Vegfa*^{iKO} retinas suggests defective pericyte
460 physiology and EC-pericyte crosstalk, as a global loss of VEGF also affects pericyte VEGFR1 signaling
461 essential for normal pericyte biology[28,29].

462 Critically, our data identify Sox17, a mechanosensitive transcription factor, as the central mediator
463 of the FSS-arterial program. Members of the SoxF family of transcription factors, Sox7, Sox17 and Sox18,
464 are expressed by all ECs[34]. Among them, only Sox17 is enriched in the arterial ECs and is implicated in
465 arterial specification[17,34]. Our data shows that Sox17 is not only a critical transcription activator for the
466 FSS-arterial program but also serves as a target for VEGF signaling to counteract the FSS-arterial
467 program. Sox18, another SoxF family member, plays only a minimal compensatory role in the Sox17-
468 mediated arterial program. These findings underscore the pivotal role of Sox17 in FSS

469 mechanotransduction pathway leading to arterial fate. Exactly how FSS mechanotransduction activates
470 Sox17 activity and how VEGF signaling opposes this effect are the subjects for further studies.
471 In conclusion, this study provides a new understanding of how vascular growth and patterning are
472 coordinated by the dynamic interaction of environmental stimuli. Transient, well controlled VEGF
473 stimulation is necessary for the formation of the capillary bed that is then partially remodeled into the
474 arterial vasculature by the FSS. The latter step, however, requires cessation of VEGF signaling. These
475 findings have direct therapeutic consideration for revascularization approaches given a dismal record of
476 unsuccessful angiogenic/arteriogenic therapies that rely on various forms of VEGF stimulation[51-54].
477
478 **Methods**
479 **Animal studies**
480 *Vegfr2*$^{flox/flox}$ mice (a gift kindly provided by Lena Claesson-Welsh, Uppsala University), *Plcg1*$^{flox/flox}$
481 mice (a gift kindly provided by Renren Wen, Wisconsin Blood Institute) and *Dll4*$^{flox/flox}$ mice (a gift kindly
482 provided by Prof. Bin Zhou, Albert Einstein College of Medicine) were crossed with *Cdh5CreER*^{T2} mice
483 (a gift kindly provided by Ralf Adams). *CBF:H2B-Venus* mice, purchased from Jackson Laboratory, were
484 crossed with *Vegfr2*$^{flox/flox}$*; Cdh5CreER*^{T2} *mice and Plcg1*$^{flox/flox}$*; Cdh5CreER*^{T2} *mice*, respectively.
485 *Vegf2*$^{flox/flox}$*; Cdh5CreER*^{T2} mice were in *C57Bl/6J* background. *Plcg1*$^{flox/flox}$*; Cdh5CreER*^{T2} *mice were*
486 *backcrossed to C57Bl/6J* background for 10 generations. Gene deletion was induced by three
487 consecutive dosages of 100μg Tamoxifen via daily peritoneal injection. Tamoxifen powder (Sigma, T5648)
488 was suspended in corn oil (Sigma, C8267) and then dissolved by agitation at 37°C for 2 hours(hrs). Rat
489 IgG or DC101 antibody was injected peritoneally at postnatal day 1 (400μg) and 3 (200μg). All
490 aforementioned mouse experimental procedures complied to the protocols approved by the Yale
491 University Institutional Animal Care and Use Committee (IACUC). Genotyping primers are listed in Table
492 S4. The following study was performed at the UCL Institute of Ophthalmology following UK Home Office
493 and institutional Animal Welfare and Ethical Review Body (AWERB) guidelines. Mice carrying the *Vegfa*$^{fl/fl}$
494 alleles[38] maintained on a mixed genetic background (C57BL6/J and 129/Sv) were crossed with *Vegfa*$^{fl/fl}$
495 mice carrying a tamoxifen-inducible *Cre* transgene under the control of the ubiquitous chicken actin
496 promoter (CAG-CreER^{TM})[55]. *Vegfa*$^{fl/fl}$ littermate pups expressing or lacking CAG-CreER^{TM} received
497 intraperitoneal injections of 50 μg tamoxifen on postnatal days (P) 2 and P4.
498
499 **Retinal dissection**
500 Mouse neonates were euthanized at postnatal day 1(P1) to 6(P6). Eyes were enucleated and
501 immediately fixed with 4% paraformaldehyde (PFA) for 8 minutes (min) at room temperature (RT). Then
502 the eyes were transferred to PBS to terminate pre-dissection fixation. Dissected retinas were fixed with
503 4% paraformaldehyde for 30 min at RT with gentle rocking, followed by 2 washes in PBS at RT, 10 min
504 each. Then retinas were dehydrated in methanol and stored at -20°C for subsequent procedure. Before
505 immunostaining, retinas stored in methanol were warmed up at room temperature and rehydrated with
506 PBS.
507
508 **Immunostaining and confocal imaging**
509 Retinas were incubated in wash buffer (PBS with 0.1%Triton X100) with gentle rocking for 15 min
510 and then in blocking buffer (wash buffer with 5% normal donkey serum (Jackson ImmunoResearch, 017-
511 000-121)) for 1-2 hrs. Blocked retinas were incubated with primary antibodies diluted in blocking buffer
512 overnight at 4°C with gentle rocking. On the next day, the retinas were washed in wash buffer for 3 times,
513 15 min each. Secondary antibodies were mixed with isolectin B4 in blocking buffer for staining at RT for
514 1.5 h with gentle rocking in dark. Staining procedure was finished after 3 washes in wash buffer, 15 min
515 each. The retinas were transferred to PBS without detergent before flat mount to slides. Antibodies and

experimental conditions were listed in Table S5. Image acquisition was conducted with Leica TCS SP8 Confocal Laser Scanning Microscope. Leica LAS-X, Image J (NIH) and IMARIS (Bitplane, USA) were used for image analysis.

EdU labeling

For in vivo EdU incorporation, 50ug EdU (Sigma #900684) solution were peritoneally injected into mouse neonates at P5 4h before retinal dissection. Erg antibody (Abcam, # ab214341) was stained to visualize endothelial nuclei, followed by detection of EdU incorporation using EdU Cell Proliferation Kit (Invitrogen, #C10340).

For In vitro experiments, EdU was added to the media to achieve a final concentration of 5uM 2 hours before cell harvesting. Click-iT™ EdU Cell Proliferation Kit for Imaging (Invitrogen, C10340) was used to detect EdU incorporation with counterstaining of DAPI.

Immunostaining of phospho-ERK1/2

Mouse neonates at P5 were placed on a warm pad at 37°C for 30min. The eyes were enucleated and immediately fixed in 4% PFA for 8 min, RT. Using ice-cold PFA will decrease fixation efficacy and must be avoided at this step. The retinas were then transferred to and dissected in ice-cold PBS. Post-dissection fixation in 4% PFA was done at 4°C with gentle rocking for 2 h. The fixed retinas were washed once with PBS for 5min, RT, and stored in ice-cold methanol at -20°C for 1 h. After warming up at RT for 15min, the retinas were rehydrated in PBS for 5min, followed by incubation in PBST (PBS with 0.25%Triton X100) for 30min and then blocking in PBST with 10% normal donkey serum (blocking buffer) for 1hr, RT. Phospho-p44/42 MAPK (Erk1/2) (Thr202/Tyr204) antibody (Cell signaling Technology, #9101) were diluted 1:100 in blocking buffer. From this step, the staining procedure followed the regular protocol described above.

Vascular perfusion assay

Mouse neonates at P5 or P6 were placed on a warm pad at 37°C for subsequent procedure of vascular perfusion. IB4-Alexa488 was diluted in PBS and retro-orbitally injected to visualize patent (lumenized) vessels. Calculation of IB4 dilution (1:50) was based on estimated blood volume 5.5ml/100g body weight (The Jackson Laboratory). 1:50= (IB4 volume) : (blood volume + injection volume). Injected pups were placed on warm pad for 20min before dissection. Dissected retinas were counter-stained with IB4-Alexa 647 to visualize all vessels, lumenized and unlumenized.

Endothelial cell culture and flow (shear stress) systems

Human microvascular blood endothelial cells (HMVBECs) (HDBECs, Promocell, #C-12211) were maintained in EGM2-MV full growth medium (Lonza). EBM2 basal medium with 5% FBS, here we term *permissive arterial differentiation medium (PADM5)*, was used for flow-induced arterial differentiation. Approximately 6 h prior to start of flow, EGM2-MV medium was removed, followed by a wash and a refill with PADM5. Human Umbilical Vein Endothelial Cells (HUVECs) (from Yale VBT) were maintained in M199 medium containing 20%FBS and endothelial cell growth supplements (ECGS, aliquots of Corning product were purchased from Yale VBT). For HUVECs, the maintenance medium was used for flow-induced arterial differentiation.

HMVBECs or HUVECs were seeded in IBIDI μ-slides (0.4 Luer ibiTreat) (IBIDI, #80176), with an initial seed density of 0.15x 10^6 (HMVBECs) or 0.12x 10^6 (HUVECs) cells per slide and were maintained for 48 h in the slide channel to reach a monolayer of homeostasis before flow experiment.

Flow system was built with a mini peristaltic pump (Cole Parmer MasterFlex Peristaltic Pump C/L drive P/N: 77122-22), an assembly of tubing systems with a syringe pulse dampener and a medium

563 reservoir. The tubing system was assembled with a coiled inlet tubing (60cm) and a coiled outlet tubing
564 (160cm), a total length of 220cm to further dampen pulsation. To avoid cell detachment, the end of the
565 outlet tubing was fit into the pump head to passively draw the flow out of the IBIDI channel instead of
566 pumping in. A flow rate of 12ml/min, which creates 12 dynes/cm^2 shear stress according to the IBIDI
567 manual, was accurately measured in each flow system prior to the start of flow experiment. Before
568 connecting IBIDI μSlides, the flow systems were placed in cell culture incubator for 30min for equilibrium
569 of temperature and CO_2.
570 To harvest cells from IBIDI μSlides for RNA or protein analysis, 150μl lysis buffer was added into the
571 channel, followed by a freezing-thawing cycle to facilitate cell lysing. To collect cell lysate from the
572 channel, approximately 75μl of thawed lysate was removed in order to create room for liquid movement.
573 Then the slide was gently tilted 10-15 times to make the rest cell lysate moving through the channel back
574 and forth. After collecting the rest cell lysate, 50ul of new lysis buffer was added into the channel and
575 then passed through repeatedly by gentle tilting to rinse off the residual cell lysate. A total of 200ul cell
576 lysate was collected from each channel.
577
578 **Small interfering RNA (siRNA) experiments**
579 FuGene SI transfection reagent (VWR, # MSPP-SI-1000) was used for siRNA transfection for lower
580 toxicity. HUVECs or HMVBECs were seeded in maintenance medium to reach a density of 80-90% on
581 the day of transfection. siRNA/FuGene/OptiMEM mix was added to EGM2-MV full growth medium for 6h,
582 followed by a wash with PBS and replacement with fresh EGM2-MV full medium. On the next day, the
583 siRNA-treated cells were trypsinized and seeded in IBIDI μSlides with maintenance medium. Flow
584 experiments started at 72h after siPLCγ1 transfection. siRNA information is listed in Table S6.
585
586 **RNA isolation and RT-qPCR**
587 Qiagen RNeasy plus Mini kit (#74134) was used for total RNA isolation, followed by reverse
588 transcription to synthesize cDNA using iScript cDNA Synthesis Kit (Bio-Rad, #170–8891). SYBR Green
589 Supermix (Bio-Rad, #1798880) was used for qPCR. Cycle threshold (Ct) values of gene expression were
590 subtracted from average housekeeping gene GAPDH, and relative quantification of experimental groups
591 versus control was calculated. QPCR primers are listed in Table S7.
592
593 **RNA sequencing and bioinformatic analysis**
594 Total RNA samples were sent to Yale Center for Genomic Analysis (YCGA) for quality analysis, library
595 preparation and sequencing. Partek Flow was used for bioinformatic analysis. Briefly, adapters in
596 RNAseq reads were trimmed, and the trimmed reads were aligned to aligner algorithm STAR. Normalized
597 gene counts were analyzed using DESeq2 to determine differential gene expression.
598
599 **Computational methods and cSTAR analysis.**
600 To analyze EC responses to FSS, VEGF and a combined FSS plus VEGF, the control condition is
601 selected as no treatment, static condition (ST) and the log fold-changes of the differentially expressed
602 genes with respect to ST were calculated. The SVM algorithm with a linear kernel from the scikit-learn
603 python library was applied to build a maximum margin hyperplane that distinguishes four different EC
604 states. The STVs are calculated as unit vectors, which are normal vectors to the three hyperplanes
605 separating EC states. After building the STVs, cSTAR calculates quantitative indicators of cell phenotypic
606 states termed DPDs. The DPD scores describe the changes in the cell phenotypic features that would
607 occur when the data point crosses on the separating hyperplanes. The absolute value of the DPD score
608 is determined by the Euclidean distances from the data point to the separating hyperplane, while the sign
609 of the DPD score indicates if the direction of the data point movement to cross the hyperplane is parallel

610 or antiparallel to the corresponding STV[24]. The DPD scores were normalized so that the DPD values in
611 the training set (FSS, VEGF, and FSS-VEGF states) were -1, 0 or 1. All codes of building STVs and
612 calculating the normalized DPD scores will be provided in a journal publication.
613
614 **Isolation of mouse retinal endothelial cell and scRNAseq**
615 Retinas of control and *PLCγ1*^{iECKO} pups at p6 were dissected in ice-cold PBS. Dissected retinas from
616 3 control and 3 *PLCγ1*^{iECKO} pups, respectively, were pooled and subjected to magnetic-activated Cell
617 sorting (MACS). Briefly, pooled retinal tissue was dissociated using Neural Tissue Dissociation kit (P)
618 (Miltenyi Biotec, Cat#130- 092-628) with gentleMACS Dissociator (Miltenyi Biotec, Cat#130- 093-235).
619 Isolated cells were suspended in PBS with 0.4% ultra-pure BSA as single cell suspension, which was
620 subsequently incubated with CD31 MicroBeads (Miltenyi Biotec, Cat#130-097-418) for 30 min at 4°C with
621 gentle rotation followed by passing through MS columns (Miltenyi Biotec, Cat#130-042-201) on an
622 OctoMACS Separator (Miltenyi Biotec, Cat#130-042-109) to enrich endothelial cells.
623 Single cell suspensions were submitted to Yale Center for Genomic Analysis (YCGA) for library
624 preparation and sequencing. scRNAseq libraries were created using Chromium GEM-X Single Cell 3′
625 Reagent Kits v4 (10x Genomics). Libraries were sequenced in NovaSeq HiSeq paired-end.
626 Reads alignment and UMI counting were conducted using the Cell Ranger software suite, with the
627 mm10 genome assembly utilized for alignment[56]. Downstream analyses, including quality control (QC)
628 filtering, batch correction, clustering, UMAP visualization, cell cycle analysis, and gene expression
629 analysis, were performed in R using Seurat v5.1[57]. For quality control, cells with mitochondrial gene
630 content exceeding 5% were excluded. Additionally, only cells with fewer than 100,000 total counts and
631 between 200 and 9,000 detected features were retained for analysis. Counts normalization was executed
632 using the Pearson residuals method implemented in the sctransform package[58]. Batch correction and
633 data integration were carried out using the RPCA approach available in Seurat package[57]. TSCAN
634 method was employed for pseudotime trajectory analysis[59]. For RNA Velocity Analysis, splicing-specific
635 counts were generated using the velocyto.py package[60]. For downstream processing of splicing data, the
636 velocyto.R and Seurat-Wrappers packages were utilized[60]. Vector field plotting was conducted using the
637 veloviz package[61] to visualize RNA velocity dynamics.
638 To access endothelial deletion of Plcg1, the brain tissue of control and *PLCγ1*^{iECKO} pups were used
639 to isolate ECs. Brain ECs were first enriched by MACS as described above, then CD31+/CD45-/PI- ECs
640 were specifically sorted out by fluorescence activated cell sorting (FACS) for RNA isolation and RT-PCR.
641 The FACS-related antibodies are summarized in Table S5. Deletion of Plcg1 in *PLCγ1*^{iECKO} ECs is
642 evidenced in Fig.S4, which demonstrates the deletion of LoxP-flanked exons2-4 and the presence of a
643 truncated Plcg1 mRNA with the downstream exons (Fig.S4b). This explains the observation of no
644 detectable decrease of Plcg1 mRNA in the *PLCγ1*^{iECKO} ECs in scRNAseq analysis (Fig.S4c), as
645 Chromium GEM-X Single Cell 3′ Reagent Kits v4 uses the poly(dT) primers that capture the polyA
646 sequences of mRNA and generates cDNA libraries with downstream sequences at the 3' end, similar to
647 a recent scRNAseq study with the same issue to detect gene deletion[62].
648
649 **Western blots**
650 The following recipe (kindly provided by Prof. Jannifer Fang, Tulane University) was used to prepare
651 10ml lysis buffer for detecting Connexins (Gja4 and Gja5) and also workable for other proteins. A tablet
652 of protease inhibitor cocktail (Roche) and a tablet of PhosSTOP were dissolved in 4.75ml water. Then
653 the following reagents were sequentially added and then mixed: 1.25ml 1M Tris, 2ml 20%SDS, 2ml
654 Glycerol, 1ml beta-mercaptoethanol and a tip amount of blumophenol blue. At the end of flow experiment,
655 IBIDI μSlides were detached from the flow system and placed on ice. To harvest protein lysate from IBIDI
656 μSlide, medium was vacuum removed from the channel and replaced with 150ul lysis buffer. To enhance

protein lysing, the IBIDI μSlide with lysis buffer was subject to a freezing-thawing cycle. Subsequently, with the removal and collection of 50% lysis buffer to create room for movement in the channel, the slide was repeatedly tilted several times to create shear force to enhance protein extraction before collecting the rest protein lysate. An additional 50ul of new lysis buffer was pipetted into the channel to rinse and collect any residual protein lysate, making a total volume of 200ul. Protein lysate was collected in a centrifuge tube and sonicated for 1 min at 15% power, followed by heating at 75°C for 30 min to denature protein. Antibodies used for western blot were listed in Table S8.

Doxycycline-induced Sox17 expression and induction of arterial differentiation

Doxycycline-inducible Sox17 expression lentiviral construct pCW57.1-hSox17-DDK-Myc was created in the Simons lab and can be shared upon reasonable request. Maintained in the aforementioned M199-based media (M199 supplemented with 20%FBS and ECGS), HUVECs at passage 2-3 were used for Lentiviral transduction, during which EGM2-MV media was temporarily used to replace M199-based media to enhance transduction efficiency and cell survival. Transduced HUVECs were selected by 0.8ug/ml puromycin in EGM2-MV media for 48 hours, followed by a 48-hour window of recovery. Puromycin-selected, transduced HUVECs were either frozen for future experiments or seeded in M199-based media for subsequent arterial differentiation experiments.

To induce arterial differentiation, 1.9-2.0 x 10^6 HUVECs harboring pCW57.1-hSox17 were seeded in M199-based media in each 10-cm dish on day1, which ensures the formation of a confluent endothelial monolayer for the start of doxycycline treatment on the next day (day2). Fresh media with doxycycline was replaced once on day3. The cells were harvested at the end of a 48-hour treatment on day4.

To ensure consistent and reproducible results, HUVECs must be regularly maintained in M199-based medium instead of EGM2, with final passage no more than 6 at the end of arterial differentiation.

Chromatin Immunoprecipitation (ChIP)

ChIP assays were conducted using SimpleChIP Plus Enzymatic Chromatin IP kit (Cell Signaling Tech #9005) following the official protocol. Briefly, HUVECs in a 10-cm dish were fixed with ultra-pure formadehyde (methanol free) (Polysciences, 18814-10) to create protein-chromatin crosslink. Immunoprecipitation was performed with antibody targeting Sox17 (CST#81778) and control rabbit IgG (CST#2729). Pull-downed chromatin was eluted, purified and assayed by QPCR.

CRISPR-cas9-mediated gene deletion

Oligos of designed gRNA sequences were cloned into lentiCRISPRv2 (Addgene #52961) following previously published protocol[63]. The following gRNA sequences were used, including a non-targeting gRNA (GTATTACTGATATTGGTGGG), a pair of gRNAs targeting human Sox17 (ACGGGTAGCCGTCGAGCGG and GGCACCTACAGCTACGCGC)[64], and a gRNA targeting human Sox18 (GTGGAAGGAGCTGAACGCGG). HUVECs transduced with lentiviral-delivered sgRNAs were selected with 0.8ug/ml puromycin for 48hrs and maintained in EGM2-MV medium for 7 days to ensure sufficient gene recombination. This was followed by a second cycle of selection with puromycin for 48hrs and recovery for 3 days before seeding the cells to the IBIDI μ slides for flow experiments.

Statistics

Data was plotted and analyzed using GraphPad Prism10. Student's t test was used for comparison of two groups, with the assumption of normal distribution and equal variance between groups. One-way or two-way ANOVA with multiple comparisons was used for grouped samples on one or two variables. A p value equal to or less than 0.05 was determined as statistically significant.

704 **Author contributions**

705 DC, MS and MAS conceptualized and designed the project. DC conducted and analyzed most of the
706 experiments. MS and MAS supervised the project. DC and MS wrote the manuscript with edits from MAS,
707 CR and KAM. OSR, DC, AT, BNK analyzed the scRNAseq data. DC analyzed the RNAseq data. OSR
708 and BNK conducted the cSTAR analysis based on the RNAseq data. DJ and BGC contributed to the
709 shear stress experiments and cloning the CRISPR-Cas9 system for Sox17 deletion and provided
710 technical assistance for DC to create the lentiviral construct of Sox17 expression. DC and RC designed
711 and conducted the Sox17 ChIP experiments with KAM's supervision. MR and EI conducted the
712 experiments of the VEGF knockout mice with CR's supervision.
713

714 **Acknowledgements**

715 We thank Prof. Lena Claesson-Welsh, Prof. Ralf Adams, Prof. Renren Wen and Genentech for
716 providing the *VEGFR2*$^{flox/flox}$, the *Cdh5CreER*^{T2}, the *PLCγ1*$^{flox/flox}$ and the *Vegfa* $^{flox/flox}$ mice, respectively.
717 We thank Dr. Hyojin Park and Dr. Eunate Gallardo for essential technical support in sample preparation
718 for single cell RNA sequencing. Sequencing service by Yale Center for Genomic Analysis reported in this
719 publication was supported by the National Institute of General Medical Sciences of the National Institutes
720 of Health under Award Number 1S10OD030363-01A1. We thank Drs. Prajwal Boddu, Emma Ristori and
721 Federico Corti for technical advice on cloning. We thank Rolando Milian, Yale Medical Library, for
722 bioinformatic training and assistance of RNAseq data analysis. We thank Tuo Guo and Guilherme Dantas
723 for technical assistance in immunostaining, confocal imaging and cloning. This work was supported by
724 NIH grants R01HL169520-01 (MS), P01HL107205-06A1 (MS and MAS), NIH/NCI grant R01CA244660
725 (BNK), EU grant no. 101136926 MULTIR (BNK), Science Foundation Ireland 22/PATH-S/10875 (OSR)
726 and Open Philanthropy (MS), British Heart Foundation PG.23.11342 (CR and MR) and PG.24.11119
727 (CR).
728

729 **Declaration of Interests**

730 The authors declare no competing interests.

731 **Reference**
732

733 1 Simons, M. & Eichmann, A. Molecular controls of arterial morphogenesis. *Circ Res* **116**, 1712-
734 1724, doi:10.1161/CIRCRESAHA.116.302953 (2015).
735 2 Gariano, R. F. & Gardner, T. W. Retinal angiogenesis in development and disease. *Nature* **438**,
736 960-966, doi:10.1038/nature04482 (2005).
737 3 Walchli, T. *et al.* Shaping the brain vasculature in development and disease in the single-cell
738 era. *Nat Rev Neurosci* **24**, 271-298, doi:10.1038/s41583-023-00684-y (2023).
739 4 Okabe, K. *et al.* Neurons limit angiogenesis by titrating VEGF in retina. *Cell* **159**, 584-596,
740 doi:10.1016/j.cell.2014.09.025 (2014).
741 5 Shweiki, D., Itin, A., Soffer, D. & Keshet, E. Vascular endothelial growth factor induced by
742 hypoxia may mediate hypoxia-initiated angiogenesis. *Nature* **359**, 843-845,
743 doi:10.1038/359843a0 (1992).
744 6 Ruhrberg, C. *et al.* Spatially restricted patterning cues provided by heparin-binding VEGF-A
745 control blood vessel branching morphogenesis. *Genes Dev* **16**, 2684-2698,
746 doi:10.1101/gad.242002 (2002).
747 7 Gerhardt, H. *et al.* VEGF guides angiogenic sprouting utilizing endothelial tip cell filopodia. *J*
748 *Cell Biol* **161**, 1163-1177, doi:10.1083/jcb.200302047 (2003).
749 8 Lobov, I. B. *et al.* Delta-like ligand 4 (Dll4) is induced by VEGF as a negative regulator of
750 angiogenic sprouting. *Proc Natl Acad Sci U S A* **104**, 3219-3224, doi:10.1073/pnas.0611206104
751 (2007).
752 9 Hellstrom, M., Phng, L. K. & Gerhardt, H. VEGF and Notch signaling: the yin and yang of
753 angiogenic sprouting. *Cell Adh Migr* **1**, 133-136, doi:10.4161/cam.1.3.4978 (2007).
754 10 Lawson, N. D. *et al.* Notch signaling is required for arterial-venous differentiation during
755 embryonic vascular development. *Development* **128**, 3675-3683 (2001).
756 11 Roca, C. & Adams, R. H. Regulation of vascular morphogenesis by Notch signaling. *Genes Dev*
757 **21**, 2511-2524, doi:10.1101/gad.1589207 (2007).
758 12 Liu, Z. J. *et al.* Regulation of Notch1 and Dll4 by vascular endothelial growth factor in arterial
759 endothelial cells: implications for modulating arteriogenesis and angiogenesis. *Mol Cell Biol* **23**,
760 14-25, doi:10.1128/MCB.23.1.14-25.2003 (2003).
761 13 Wythe, J. D. *et al.* ETS factors regulate Vegf-dependent arterial specification. *Dev Cell* **26**, 45-
762 58, doi:10.1016/j.devcel.2013.06.007 (2013).
763 14 Duarte, A. *et al.* Dosage-sensitive requirement for mouse Dll4 in artery development. *Genes*
764 *Dev* **18**, 2474-2478, doi:10.1101/gad.1239004 (2004).
765 15 Hasan, S. S. *et al.* Endothelial Notch signalling limits angiogenesis via control of artery
766 formation. *Nat Cell Biol* **19**, 928-940, doi:10.1038/ncb3574 (2017).
767 16 Pitulescu, M. E. *et al.* Dll4 and Notch signalling couples sprouting angiogenesis and artery
768 formation. *Nat Cell Biol* **19**, 915-927, doi:10.1038/ncb3555 (2017).
769 17 Corada, M. *et al.* Sox17 is indispensable for acquisition and maintenance of arterial identity. *Nat*
770 *Commun* **4**, 2609, doi:10.1038/ncomms3609 (2013).
771 18 Hellstrom, M. *et al.* Dll4 signalling through Notch1 regulates formation of tip cells during
772 angiogenesis. *Nature* **445**, 776-780, doi:10.1038/nature05571 (2007).
773 19 Benedito, R. *et al.* Loss of Notch signalling induced by Dll4 causes arterial calibre reduction by
774 increasing endothelial cell response to angiogenic stimuli. *BMC Dev Biol* **8**, 117,
775 doi:10.1186/1471-213X-8-117 (2008).
776 20 Suchting, S. *et al.* The Notch ligand Delta-like 4 negatively regulates endothelial tip cell
777 formation and vessel branching. *Proc Natl Acad Sci U S A* **104**, 3225-3230,
778 doi:10.1073/pnas.0611177104 (2007).
779 21 Fang, J. S. *et al.* Shear-induced Notch-Cx37-p27 axis arrests endothelial cell cycle to enable
780 arterial specification. *Nat Commun* **8**, 2149, doi:10.1038/s41467-017-01742-7 (2017).
781 22 Mack, J. J. *et al.* NOTCH1 is a mechanosensor in adult arteries. *Nat Commun* **8**, 1620,
782 doi:10.1038/s41467-017-01741-8 (2017).

23 Kholodenko, B. N., Kolch, W. & Rukhlenko, O. S. Reversing pathological cell states: the road less travelled can extend the therapeutic horizon. *Trends Cell Biol* **33**, 913-923, doi:10.1016/j.tcb.2023.04.004 (2023).
24 Rukhlenko, O. S. *et al.* Control of cell state transitions. *Nature* **609**, 975-985, doi:10.1038/s41586-022-05194-y (2022).
25 Yabaji, S. M. *et al.* Cell state transition analysis identifies interventions that improve control of Mycobacterium tuberculosis infection by susceptible macrophages. *Sci Adv* **9**, eadh4119, doi:10.1126/sciadv.adh4119 (2023).
26 Stahl, A. *et al.* The mouse retina as an angiogenesis model. *Invest Ophthalmol Vis Sci* **51**, 2813-2826, doi:10.1167/iovs.10-5176 (2010).
27 Pontes-Quero, S. *et al.* High mitogenic stimulation arrests angiogenesis. *Nat Commun* **10**, 2016, doi:10.1038/s41467-019-09875-7 (2019).
28 Donoghue, L., Tyburski, J. G., Steffes, C. P. & Wilson, R. F. Vascular endothelial growth factor modulates contractile response in microvascular lung pericytes. *Am J Surg* **191**, 349-352, doi:10.1016/j.amjsurg.2005.10.034 (2006).
29 Eilken, H. M. *et al.* Pericytes regulate VEGF-induced endothelial sprouting through VEGFR1. *Nat Commun* **8**, 1574, doi:10.1038/s41467-017-01738-3 (2017).
30 Kilarski, W. W., Samolov, B., Petersson, L., Kvanta, A. & Gerwins, P. Biomechanical regulation of blood vessel growth during tissue vascularization. *Nat Med* **15**, 657-664, doi:10.1038/nm.1985 (2009).
31 Tong, R. T. *et al.* Vascular normalization by vascular endothelial growth factor receptor 2 blockade induces a pressure gradient across the vasculature and improves drug penetration in tumors. *Cancer Res* **64**, 3731-3736, doi:10.1158/0008-5472.CAN-04-0074 (2004).
32 Takahashi, T., Yamaguchi, S., Chida, K. & Shibuya, M. A single autophosphorylation site on KDR/Flk-1 is essential for VEGF-A-dependent activation of PLC-gamma and DNA synthesis in vascular endothelial cells. *EMBO J* **20**, 2768-2778, doi:10.1093/emboj/20.11.2768 (2001).
33 Chen, D. & Simons, M. Emerging roles of PLCgamma1 in endothelial biology. *Sci Signal* **14**, doi:10.1126/scisignal.abc6612 (2021).
34 Zhou, Y., Williams, J., Smallwood, P. M. & Nathans, J. Sox7, Sox17, and Sox18 Cooperatively Regulate Vascular Development in the Mouse Retina. *PLoS One* **10**, e0143650, doi:10.1371/journal.pone.0143650 (2015).
35 Raza, Q. *et al.* Notch signaling regulates UNC5B to suppress endothelial proliferation, migration, junction activity, and retinal plexus branching. *Sci Rep* **14**, 13603, doi:10.1038/s41598-024-64375-z (2024).
36 Nornes, S., Bruche, S., Adak, N., McCracken, I. & Val, S. D. A catalogue of verified and characterized arterial enhancers for key arterial identity genes. *bioRxiv*, 2024.2004.2030.591717, doi:10.1101/2024.04.30.591717 (2024).
37 Geudens, I. & Gerhardt, H. Coordinating cell behaviour during blood vessel formation. *Development* **138**, 4569-4583, doi:10.1242/dev.062323 (2011).
38 Gerber, H. P. *et al.* VEGF is required for growth and survival in neonatal mice. *Development* **126**, 1149-1159, doi:10.1242/dev.126.6.1149 (1999).
39 Apte, R. S., Chen, D. S. & Ferrara, N. VEGF in Signaling and Disease: Beyond Discovery and Development. *Cell* **176**, 1248-1264, doi:10.1016/j.cell.2019.01.021 (2019).
40 Red-Horse, K. & Siekmann, A. F. Veins and Arteries Build Hierarchical Branching Patterns Differently: Bottom-Up versus Top-Down. *Bioessays* **41**, e1800198, doi:10.1002/bies.201800198 (2019).
41 Corti, F. *et al.* N-terminal syndecan-2 domain selectively enhances 6-O heparan sulfate chains sulfation and promotes VEGFA(165)-dependent neovascularization. *Nat Commun* **10**, 1562, doi:10.1038/s41467-019-09605-z (2019).
42 Cudmore, M. J. *et al.* The role of heterodimerization between VEGFR-1 and VEGFR-2 in the regulation of endothelial cell homeostasis. *Nat Commun* **3**, 972, doi:10.1038/ncomms1977 (2012).

43 Kendall, R. L., Wang, G. & Thomas, K. A. Identification of a natural soluble form of the vascular endothelial growth factor receptor, FLT-1, and its heterodimerization with KDR. *Biochem Biophys Res Commun* **226**, 324-328, doi:10.1006/bbrc.1996.1355 (1996).
44 Rahimi, N., Dayanir, V. & Lashkari, K. Receptor chimeras indicate that the vascular endothelial growth factor receptor-1 (VEGFR-1) modulates mitogenic activity of VEGFR-2 in endothelial cells. *J Biol Chem* **275**, 16986-16992, doi:10.1074/jbc.M000528200 (2000).
45 Dixelius, J. *et al.* Ligand-induced vascular endothelial growth factor receptor-3 (VEGFR-3) heterodimerization with VEGFR-2 in primary lymphatic endothelial cells regulates tyrosine phosphorylation sites. *J Biol Chem* **278**, 40973-40979, doi:10.1074/jbc.M304499200 (2003).
46 Shay-Salit, A. *et al.* VEGF receptor 2 and the adherens junction as a mechanical transducer in vascular endothelial cells. *Proc Natl Acad Sci U S A* **99**, 9462-9467, doi:10.1073/pnas.142224299 (2002).
47 Coon, B. G. *et al.* Intramembrane binding of VE-cadherin to VEGFR2 and VEGFR3 assembles the endothelial mechanosensory complex. *J Cell Biol* **208**, 975-986, doi:10.1083/jcb.201408103 (2015).
48 Tzima, E. *et al.* A mechanosensory complex that mediates the endothelial cell response to fluid shear stress. *Nature* **437**, 426-431, doi:10.1038/nature03952 (2005).
49 Somanath, P. R., Malinin, N. L. & Byzova, T. V. Cooperation between integrin alphavbeta3 and VEGFR2 in angiogenesis. *Angiogenesis* **12**, 177-185, doi:10.1007/s10456-009-9141-9 (2009).
50 le Noble, F. & Kupatt, C. Interdependence of Angiogenesis and Arteriogenesis in Development and Disease. *Int J Mol Sci* **23**, doi:10.3390/ijms23073879 (2022).
51 Isner, J. M. *et al.* Arterial gene therapy for therapeutic angiogenesis in patients with peripheral artery disease. *Circulation* **91**, 2687-2692, doi:10.1161/01.cir.91.11.2687 (1995).
52 Rajagopalan, S. *et al.* Regional angiogenesis with vascular endothelial growth factor in peripheral arterial disease: a phase II randomized, double-blind, controlled study of adenoviral delivery of vascular endothelial growth factor 121 in patients with disabling intermittent claudication. *Circulation* **108**, 1933-1938, doi:10.1161/01.CIR.0000093398.16124.29 (2003).
53 Iyer, S. R. & Annex, B. H. Therapeutic Angiogenesis for Peripheral Artery Disease: Lessons Learned in Translational Science. *JACC Basic Transl Sci* **2**, 503-512, doi:10.1016/j.jacbts.2017.07.012 (2017).
54 Stewart, D. J. *et al.* VEGF gene therapy fails to improve perfusion of ischemic myocardium in patients with advanced coronary disease: results of the NORTHERN trial. *Mol Ther* **17**, 1109-1115, doi:10.1038/mt.2009.70 (2009).
55 Hayashi, S. & McMahon, A. P. Efficient recombination in diverse tissues by a tamoxifen-inducible form of Cre: a tool for temporally regulated gene activation/inactivation in the mouse. *Dev Biol* **244**, 305-318, doi:10.1006/dbio.2002.0597 (2002).
56 Zheng, G. X. *et al.* Massively parallel digital transcriptional profiling of single cells. *Nat Commun* **8**, 14049, doi:10.1038/ncomms14049 (2017).
57 Hao, Y. *et al.* Dictionary learning for integrative, multimodal and scalable single-cell analysis. *Nat Biotechnol* **42**, 293-304, doi:10.1038/s41587-023-01767-y (2024).
58 Hafemeister, C. & Satija, R. Normalization and variance stabilization of single-cell RNA-seq data using regularized negative binomial regression. *Genome Biol* **20**, 296, doi:10.1186/s13059-019-1874-1 (2019).
59 Ji, Z. & Ji, H. TSCAN: Pseudo-time reconstruction and evaluation in single-cell RNA-seq analysis. *Nucleic Acids Res* **44**, e117, doi:10.1093/nar/gkw430 (2016).
60 La Manno, G. *et al.* RNA velocity of single cells. *Nature* **560**, 494-498, doi:10.1038/s41586-018-0414-6 (2018).
61 Atta, L., Sahoo, A. & Fan, J. VeloViz: RNA velocity-informed embeddings for visualizing cellular trajectories. *Bioinformatics* **38**, 391-396, doi:10.1093/bioinformatics/btab653 (2022).
62 Zarkada, G. *et al.* Specialized endothelial tip cells guide neuroretina vascularization and blood-retina-barrier formation. *Dev Cell* **56**, 2237-2251 e2236, doi:10.1016/j.devcel.2021.06.021 (2021).
63 Sanjana, N. E., Shalem, O. & Zhang, F. Improved vectors and genome-wide libraries for CRISPR screening. *Nat Methods* **11**, 783-784, doi:10.1038/nmeth.3047 (2014).

889 64 Jostes, S. V. *et al.* Unique and redundant roles of SOX2 and SOX17 in regulating the germ cell
890 tumor fate. *Int J Cancer* **146**, 1592-1605, doi:10.1002/ijc.32714 (2020).
891

Figure 1. VEGF-A counteracts FSS-driven capillary-to-artery cell state transition.

a. RNAseq differential gene expression clustering analysis of arterial and capillary genes. HMVBECs were cultured in the conditions of static (ST), VEGF (20ng/ml), FSS (12dyn/cm^2) and FSS+VEGF for 16 hours. Gene expression matrix is demonstrated by both color intensity and size. **b-c.** Validation of the arterial and capillary genes by quantitative RT-PCR (**b**) and western blot (**c**). **d.** Western blot results of HMVBECs cultured in the conditions of ST, FSS with a gradient of VEGF (0, 2, 10, 20ng/ml). **e.** Western blot results of HMVBECs treated with a gradient of FSS with and without VEGF. **b-e.** One-way ANOVA with multiple comparisons was used for statistics. A p value equal to or less than 0.05 was determined as statistically significant, in extents demonstrated by asterisks * ($p \leqslant 0.05$), ** ($p \leqslant 0.01$), *** ($p \leqslant 0.001$), **** ($p \leqslant 0.0001$). ns: not significant.

f. cSTAR analysis of RNAseq data. DPD scores of EC states shown in 3D space of the STV_{FSS}, STV_{VEGF}, and STV_{SSVA}. Four EC states correspond to different FSS and VEGF treatments. A change in the EC phenotype is quantified by the DPD score along the corresponding STV. The first cSTAR step uses a machine learning technique called support vector machines (SVM) to exploit the high-dimensional transcriptomics space and construct separating surfaces between distinct EC states. Subsequently, the directions of EC state conversions are determined in the transcriptomic space. These directions are the shortest paths from one EC state to another state, which are specified by the State Transition Vectors (STVs). STVs are unit vectors defined as normal vectors to the hyperplanes that separate EC phenotypic states. After building the STVs, cSTAR calculates quantitative indicators of cell phenotypic states termed Dynamic Phenotype Descriptors (DPD). For EC cells in different states, the DPD scores describe phenotypic features associated with each STV[28,29]. The STV_{FSS} indicates the shortest path from an EC ST state to a FSS state, and the DPD_{FSS} quantifies a normalized FSS-related score of the changes in the transcriptomics patterns. The STV_{VEGF} indicates the direction from an ST state to a new EC state caused by VEGF stimulation at zero FSS, whereas the DPD_{VEGF} scores quantify the extent of the transcriptomics changes related to VEGF stimulation. The angle between two directions of the transcriptomics changes, STV_{FSS} and STV_{VEGF} is 84 degrees. The near orthogonality of these two STVs suggests mutually independent transcriptomic changes between the FSS and VEGF EC states, with any slight deviation from orthogonality indicating a minor overlap in the regulatory pathways induced by FSS or VEGF. To better understand changes in the transcriptomic profile of the FSS EC state brought about by VEGF stimulation, we built the STV_{SSVA} to determine the direction of the EC FSS state change induced by a combined FSS and VEGF stimulation. The resulting STV_{SSVA} appears to be almost orthogonal to both STVs determined above (the angle between the two vectors, STV_{SSVA} and STV_{FSS} is 89 degrees, and the angle between the STV_{SSVA} and the STV_{VEGF} is 87 degrees suggesting that this combination (VEGF+FSS) leads to a new state distinct from both STV_{VEGF} and $STV_{FSS.}$ Based on the STV_{SSVA}, we next calculated the DPD_{SSVA} that scores the changes in the phenotypic cell features following combined FSS and VEGF treatment. A combined VEGF and FSS treatment only slightly increases the DPD_{VEGF} score of the FSS state and does not change the DPD_{FSS} score.

Figure 2. Arteriogenesis takes place in the capillary regions with declined VEGF activity.

a. Formation and remodeling of the capillary bed in mouse postnatal retina. Mouse retinas were dissected at P1-4, followed by immunostaining of Sox17 and IB4. The arrow in P2 indicates emergence of arterial morphogenesis labeled by high level of Sox17 expression. The gray arrow on the right indicates the direction of vascular expansion from the retinal center to the periphery. The yellow dashed lines in the bottom panel represent the dynamic movement of the vascular fronts visualized in the top panel. **b.** VEGF activities and blood flow in P5 retina. i.v.: intravenous (retro-orbital) injection. **c.** A

stereotypic vasculature at P5 with immunostaining of Sox17 and IB4. The arrows demonstrate arterial and post-arterial blood flow, from the artery to the un-arterialized artery associated capillary (defined here as Arterial Delta). The right bars demonstrate the gradients of VEGF and FSS. Abbreviations: A: artery; V: vein. Scale bars: 100μm.

Figure 3: VEGF signaling is not required for arterial specification during capillary remodeling.
a-b. Mouse neonatal retinas dissected at p6, followed by immunostaining of IB4 and antibodies targeting Sox17 and SMA. Yellow dashed lines indicate the vascular front. White dashed brackets indicate the un-arterialized gap between Sox17-labeled arterial tip and the vascular front. **a**. Control and *Vegfa*^{iKO} retinas dissected at p6. Arrow heads indicate ectopic arterialization (EA). **b**. Control and *Vegfr2*^{iECKO} retinas dissected at p6. Blue dashed rectangles in the quantification plots per artery indicate the arteries with full extension and no un-arterialized gap from the artery tip to the vascular front. Abbreviations: A: artery; EA: ectopic arterialization; V: vein. UG: un-arterialized gap. Scale bars: 500 μm (the left columns in a-d); 100μm (the right 3 columns in a-d). Two tailed, unpaired Student t-test was used for statistics. A p value equal to or less than 0.05 was determined as statistically significant, in extents demonstrated by asterisks * ($p \leqslant 0.05$), ** ($p \leqslant 0.01$), *** ($p \leqslant 0.001$), **** ($p \leqslant 0.0001$). Numeric values are reported for p values greater than 0.05.
c. Control and *VEGFR2*^{iECKO} retinas immunostained with IB4 and VEGFR2 to visualize endothelial-specific deletion of VEGFR2. The areas in the white dashed squares are shown in higher magnification in the images of the next column. White arrow heads indicate Sox17^{high}/VEGFR2^{+} ECs in the control mice. Blue arrow heads indicate Sox17^{high}/VEGFR2^{null} ECs. Abbreviations: A: artery; V: vein. Scale bars: 300μm(a), 100μm (b and c).

Figure 4: Blocking VEGF signaling leads to ectopic arterialization in the Arterial Delta region.
Mouse neonatal retinas dissected at p6, followed by immunostaining of IB4 and antibodies targeting Sox17 and SMA. Yellow dashed lines indicate the vascular front. White dashed brackets indicate the un-arterialized gap between Sox17-labeled arterial tip and the vascular front. **a.** Retinas from pups treated with two doses of IgG or DC101 antibody injection at p1 (400μg) and p3(200μg). **b**. Control and *Plcg1*^{iECKO} retinas (tamoxifen induction of gene deletion at p1-3). Blue dashed rectangles in the quantification plots per artery indicate the arteries with full extension and no un-arterialized gap from the artery tip to the vascular front. Arrow heads indicate ectopic arterialization (EA). Abbreviations: A: artery; EA: ectopic arterialization; V: vein. UG: un-arterialized gap. Scale bars: 500 μm (the left columns in a-d); 100μm (the right 3 columns in a-d). Two tailed, unpaired Student t-test was used for statistics. A p value equal to or less than 0.05 was determined as statistically significant, in extents demonstrated by asterisks * ($p \leqslant 0.05$), ** ($p \leqslant 0.01$), *** ($p \leqslant 0.001$), **** ($p \leqslant 0.0001$). Numeric values are reported for p values greater than 0.05.

Figure 5: Fluid shear stress-induced arterial program is independent of VEGFR2 signaling.
a. Mouse postnatal retinas were dissected at p6. Before dissection, IB4 (green, IB4-iv) was retro-orbitally injected to perfuse the retina vasculatures of Control, DC101-treated, *Vegfr2*^{iECKO} and *Plcg1*^{iECKO} mice. Dissected retinas were stained with IB4 (red) to visualize all perfused and non-perfused blood vessels. Perfused vessels are double-stained (IB4-green/red), while vessels not perfused were single-stained (IB4-red only, indicated by white arrow heads). Abbreviations: i.v.: intravenous (retro-orbital) injection. A: artery; V: vein. Scale bars: 100μm. **b**. HUVECs with siPLCg1 treatments were subjected to static (ST) or FSS (12dyn/cm^2) for 16 hours to induce arterial differentiation. Gene expression was examined by quantitative RT-PCR followed by quantification

relative to ST-siCTRL. Two-way ANOVA with multiple comparisons was used for statistics. A p value equal to or less than 0.05 was determined as statistically significant, in extents demonstrated by asterisks * ($p \leqslant 0.05$), ** ($p \leqslant 0.01$). ns: not significant. Error bars indicate standard error of the mean.

Figure 6: Blocking VEGFR2 signaling promotes capillary-to-artery transition in scRNAseq.
a. Arteriovenous zonation in combined control and *Plcg1*^{iECKO} retinal ECs. **b**. Distributions of control and *Plcg1*^{iECKO} retinal ECs in clusters 0-9. Quantification plots demonstrating percentage and log2 fold change of the cells in clusters 0-9 in control and *Plcg1*^{iECKO}. **c**. Pseudotime trajectory analysis by TSCAN. **d.** RNA velocity analysis demonstrating transitioning trajectories of control and *Plcg1*^{iECKO} retinal ECs.

Figure 7: Sox17 is a mechanosensitive transcription factor essential for the FSS-induced arterial program.
a. HUVECs lentivirally transduced with CRISPR-Cas9-directed sgNT, sgSox17, sgSox18 or combined sgSox17/18 were used to test FSS-induced arterial differentiation. Cell lysates were analyzed by western blot. **b.** HUVECs harboring a doxycycline-inducible Sox17 expression system (pCW57.1-hSox17-myc-DDK) were treated by a gradient of doxycycline (DOX) for 48 hours. Cell lysates were analyzed by western blot. One-way ANOVA with multiple comparisons was used for statistics. A p value equal to or less than 0.05 was determined as statistically significant, in extents demonstrated by asterisks * ($p \leqslant 0.05$), ** ($p \leqslant 0.01$), *** ($p \leqslant 0.001$), **** ($p \leqslant 0.0001$). ns: not significant.

Figure 8: VEGF antagonizes Sox17 transcription activity on arterial promoters and enhancers.
a-c. HUVECs harboring a doxycycline-inducible Sox17 expression system (pCW57.1-hSox17-myc-DDK) were used for these experiments for 48 hours. **a.** Quantitative RT-PCR analysis of RNA expression under experimental conditions of no treatment (NT), DOX (1000ng/ml) and DOX (1000ng/ml)+VEGF (50ng/ml). Definitive arterial genes (Gja5, Gja4, Sema3g, Jag1, Cxcl12 and Efnb2) and VEGF-Notch (V-N) targets (Unc5b and Dll4) were tested. **b.** A dose gradient of VEGF (0-100ng/ml) was used to test the impact on DOX-induced arterial differentiation. Cell lysates were analyzed by western blot. **c.** Chromatin immunoprecipitation (ChIP) results of Sox17 enrichment on the promoters and enhancers of the definitive arterial genes. The results are demonstrated by fold changes of percentage input relative to NT. **d.** Working model: VEGF signaling counteracts FSS-induced arterial specification by compromising Sox17-mediated transcription regulation. Gja4 is used as an example in this diagram. Left: in the absence of VEGF signaling, FSS-induced Sox17 is enriched at its binding motifs on arterial promoters and enhancers, forming an activating transcription complex to turn on arterial gene expression. Right: VEGF signaling compromises the enrichment of Sox17 on arterial promoters and enhancers, thereby turning off the expression of arterial gene. One-way ANOVA with multiple comparisons was used for statistics. A p value equal to or less than 0.05 was determined as statistically significant, in extents demonstrated by asterisks * ($p \leqslant 0.05$), ** ($p \leqslant 0.01$), *** ($p \leqslant 0.001$), **** ($p \leqslant 0.0001$). ns: not significant.

Figure 9: Angiogenic signaling is a physiological brake to counteract FSS-driven arteriogenesis.
a. VEGF and FSS counteract to control angiogenesis and arteriogenesis from the capillary bed. The condition with high level of VEGF and low FSS favors angiogenesis and inhibits arteriogenesis, while arteriogenesis requires a decline of VEGF signaling as a permissive prerequisite to allow high arterial level of FSS to drive arterial specification. **b.** Artistic modeling of postnatal retinal vascular morphogenesis under physiological condition or blocked VEGFR2 signaling. Red arrows indicate the

directionality of arterial (dark red) and post-arterial (light red) FSS. Blue arrows indicate the directionality of pre-venous (light blue) and venous (dark blue) FSS. The shaded artery-associated capillary area between the arterial tip and the vascular front is defined as the "*Arterial Delta*" in this study. Exposed to effective post-arterial FSS from the artery and high level of VEGF diffused from the juxtaposed avascular zone, the un-arterialized Arterial Delta region of capillary is where VEGF-FSS competition takes place. Blocking VEGF signaling removes the physiological brake that counteracts the FSS-induced arterial program, leaving FSS as the sole player that ectopically arterializes the Arterial Delta and beyond.

Fig.S1. VEGF-FSS crosstalk regulates arterial specification in HUVECs.
HUVECs were subjected to the conditions of static (VEGF-/FSS-), ST with 20ng/ml VEGF (VEGF+/FSS-), 12dyn/cm^2 FSS (FSS+/VEGF-) and FSS+VEGF (FSS+/VEGF+). Cell lyasates were analyzed by western blot. While most definitive arterial genes responded to VEGF and VEGF+FSS the same manner as HMVBECs (Fig.1), FSS induction of Sox17 in HUVECs is further promoted by VEGF. One-way ANOVA with multiple comparisons was used for statistics. A p value equal to or less than 0.05 was determined as statistically significant, in extents demonstrated by asterisks * ($p \leqslant 0.05$), ** ($p \leqslant 0.01$). ns: not significant.

Fig.S2. Endothelial deletion of PLCγ1 in P6 mouse neonates.
a. A demonstration of the exons in mouse PLCg1 gene in control and *Plcg1^{iECKO}*. Two loxP sites flank exons 2-4, which are excised in *Plcg1^{iECKO}*. Two sets of PCR primers were designed to detect Exons2-3 (Ex2-3) or downstream Exons 24-26 (Ex24-26). **b.** Pool brains from control and *PLCγ1^{iECKO}* pups at P6 (tamoxifen induction at P1-3) were first enriched by magnetic activated cell sorting (MACS) and further sorted by Fluorescence-activated cell sorting (FACS) in flow cytometry sorting out the CD31+ (APC)/CD45- (BV421)/PI- (PE) ECs. Plcg1 mRNA was detected by primer sets for Ex2-3 or Ex24-26. **c.** Distribution of retinal ECs with Plcg1 RNA expression in GEM-X 3' scRNAseq.

Fig.S3. Clustering of endothelial cells in a single-cell transcriptome.
30 clusters of cells from control and *Plcg1^{iECKO}* retinas were identified and demonstrated in UMAP. Endothelial cells in cluster 12 were identified by high expression levels of Pecam1, Cdh5 and Cldn5.

Fig.S4. Mapping arteriovenous zonation in a single cell transcriptome.
a. Identification of clusters 0-9 in all combined control and *Plcg1^{iECKO}* endothelial cells. **b.** Cluster 6 enriched with Esm1 and Kcne3 is identified as sprouting ECs. **c-d.** The cells in Cluster 9 expressing high level of arterial markers are arterial ECs. Clusters 0, 2, 3, 4, 6, 7 are identified as capillary/venous clusters. The cells in Cluster 8 are arterial predecessors with both arterial and capillary profiles. The ECs in Cluster 1 have weak capillary identity. **e.** The ECs in Cluster5 express low levels of endothelial markers, likely losing endothelial identity. **f.** Mapping cell cycle. Cluster 0 identified as proliferative capillary ECs mostly in G2/M phase.

Fig.S5 VEGF does not significantly alter FSS-induced cell cycle arrest.
a. RNAseq differential gene expression clustering analysis of cell cycle regulators. HMVBECs were cultured in the conditions of static (ST), VEGF (20ng/ml), FSS (12dyn/cm^2) and FSS+VEGF for 16 hours. Gene expression matrix is demonstrated by both color intensity and size. **b.** Validation of the arterial and capillary genes by quantitative RT-PCR. **c.** EdU incorporation assay. 5uM EdU was added to the media 2 hours before cell harvesting.

Fig.S6. VEGF does not use Notch to counteract the FSS-induced arterial program.
Pretreated with DMSO or 5uM DAPT for 3h, HMVBECs were harvested (FSS 0 hr) or subjected to FSS with DMSO or DAPT for 16 hr. Samples were analyzed by western blot. One-way ANOVA with multiple comparisons was used for statistics. A p value equal to or less than 0.05 was determined as statistically significant, in extents demonstrated by asterisks * ($p \leqslant 0.05$), ** ($p \leqslant 0.01$). ns: not significant.

Table S1. Endothelial markers for mapping arteriovenous zonation.

Table S2. A matrix of the DPD scores.

Table S3. Predicted transcription factor binding motifs of Sox17 and RBPJ in arterial and capillary genes (TRANSFACT).

Table S4. Genotyping primers

Table S5. Antibodies for immunostaining.

Table S6. siRNA information.

Table S7. QPCR primers

Table S8. Antibodies for western blot.

Table S9. QPCR primers for ChIP.

Fig.1 VEGF-A counteracts FSS-driven capillary-to-artery cell state transition.

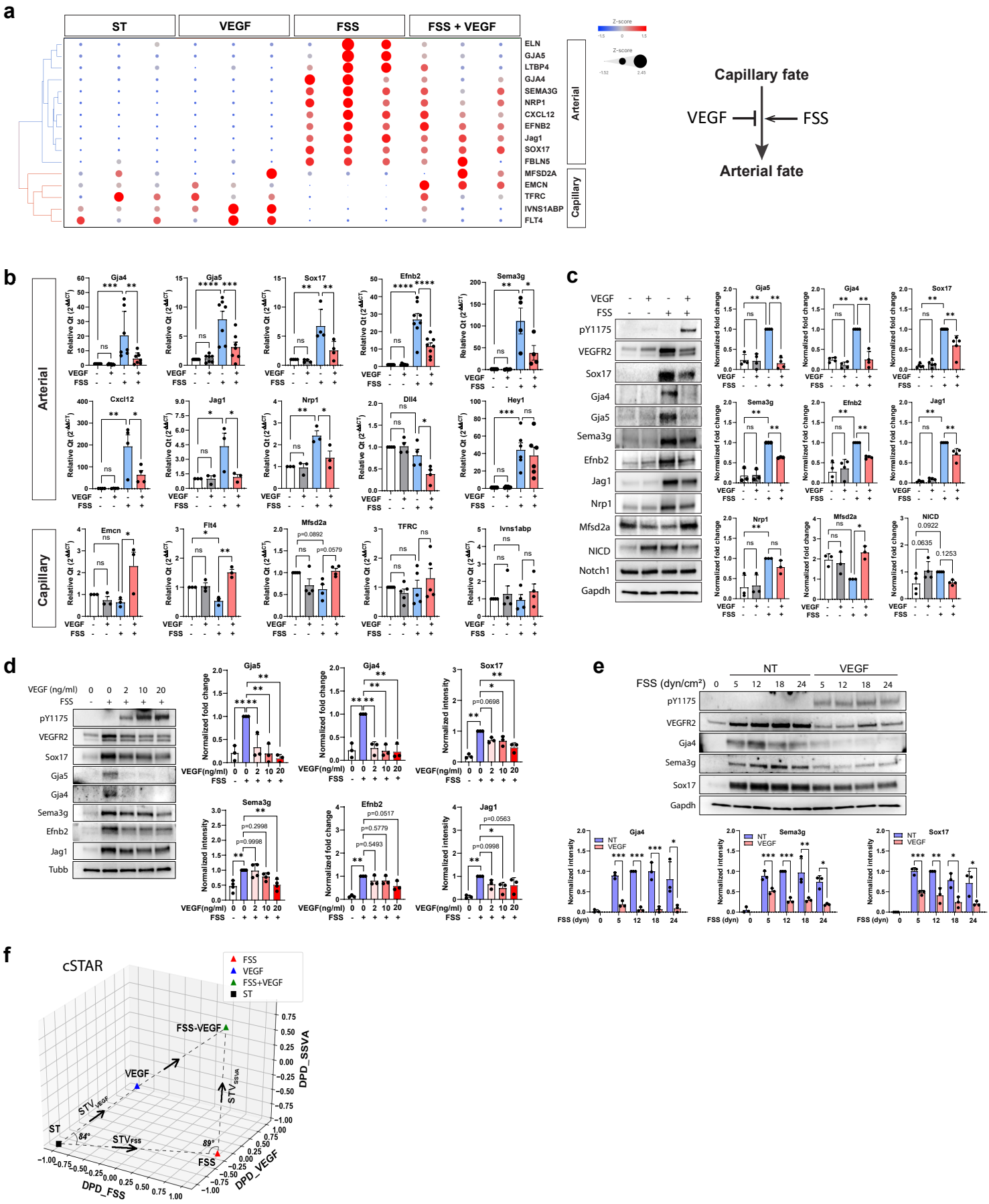

Fig.2. Arteriogenesis takes place in the capillary regions with declined VEGF activity.

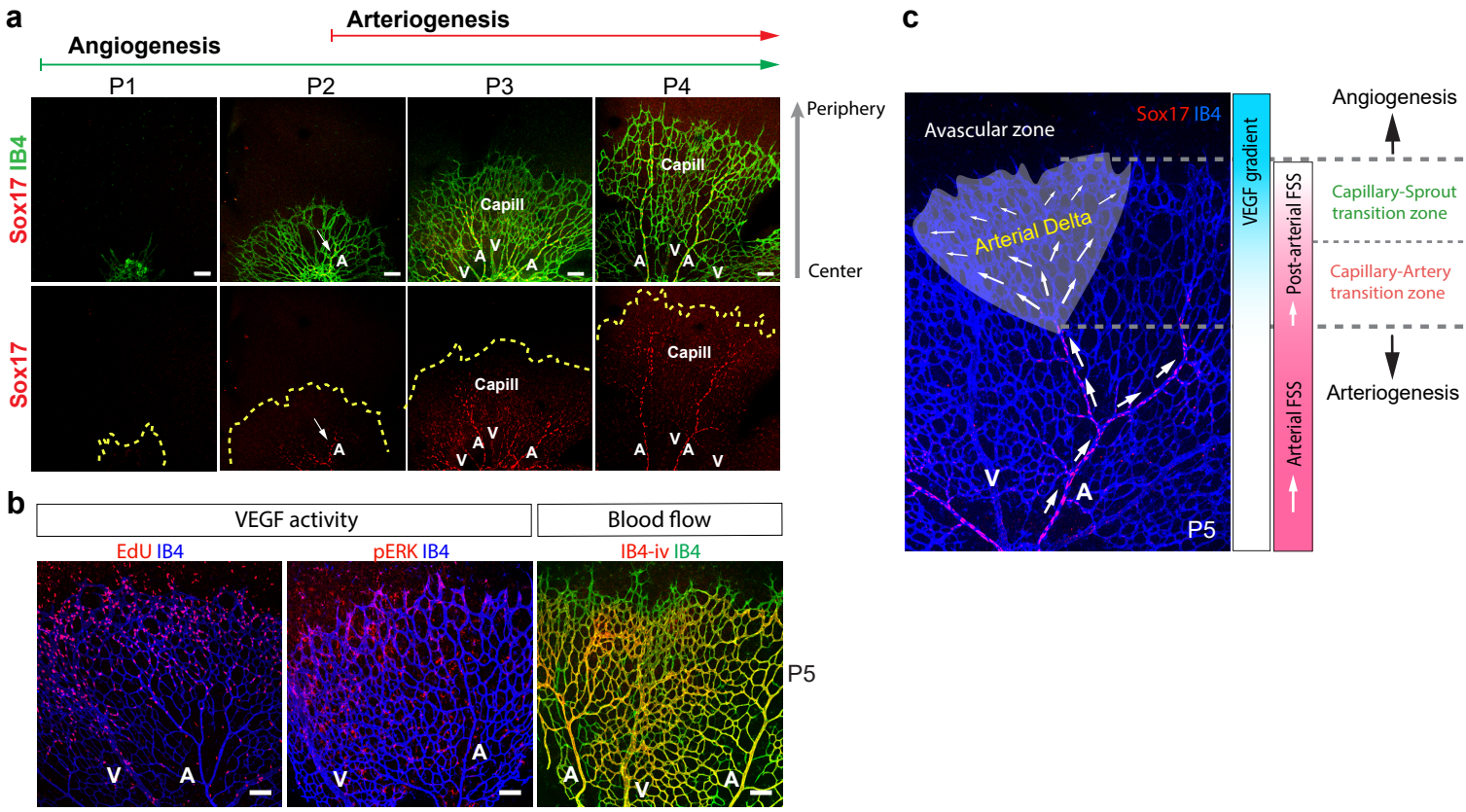

Fig.3 VEGF signaling is not required for arterial specification during capillary remodeling.

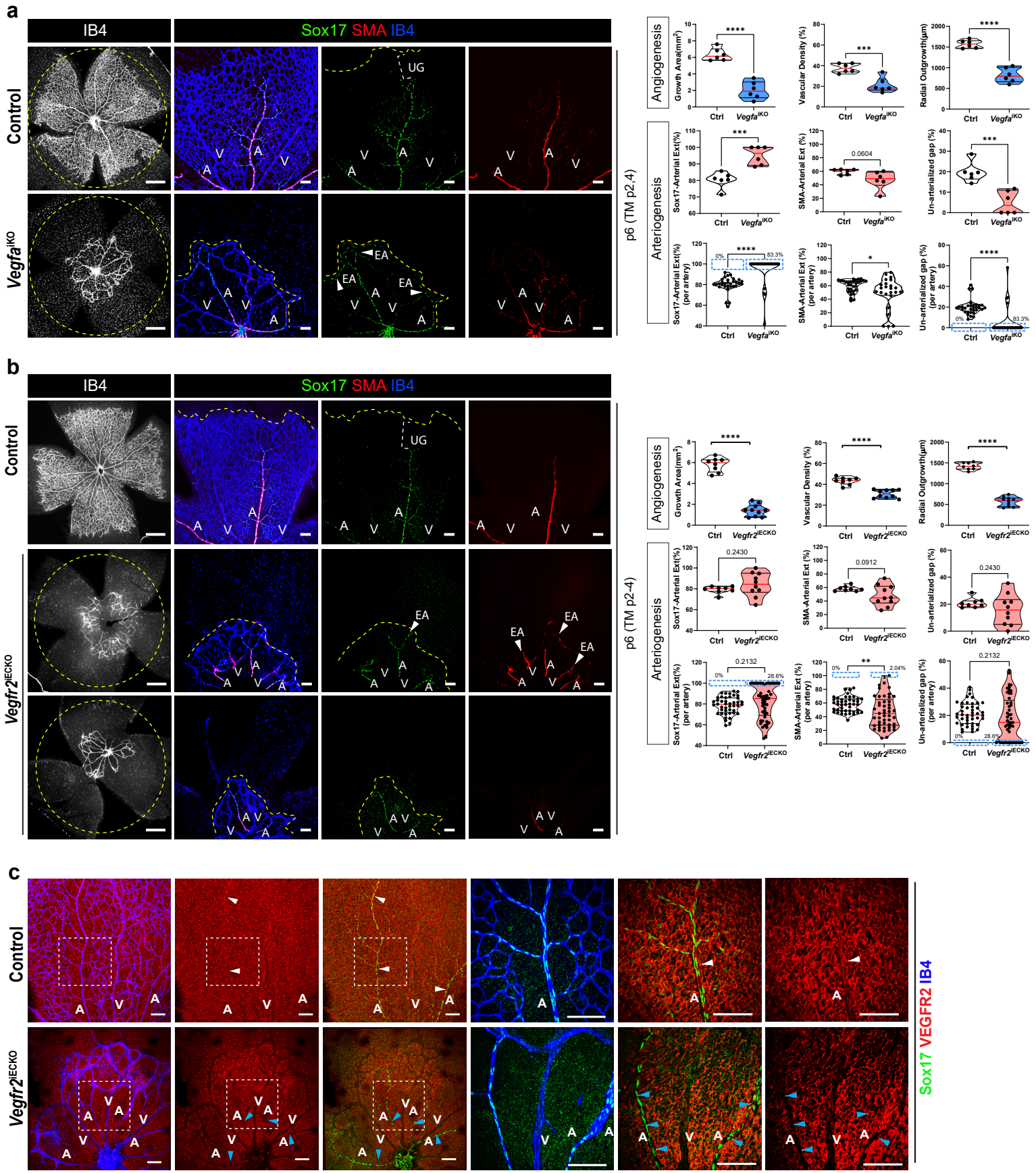

Fig.4 Blocking VEGF signaling leads to ectopic arterialization in the Arterial Delta.

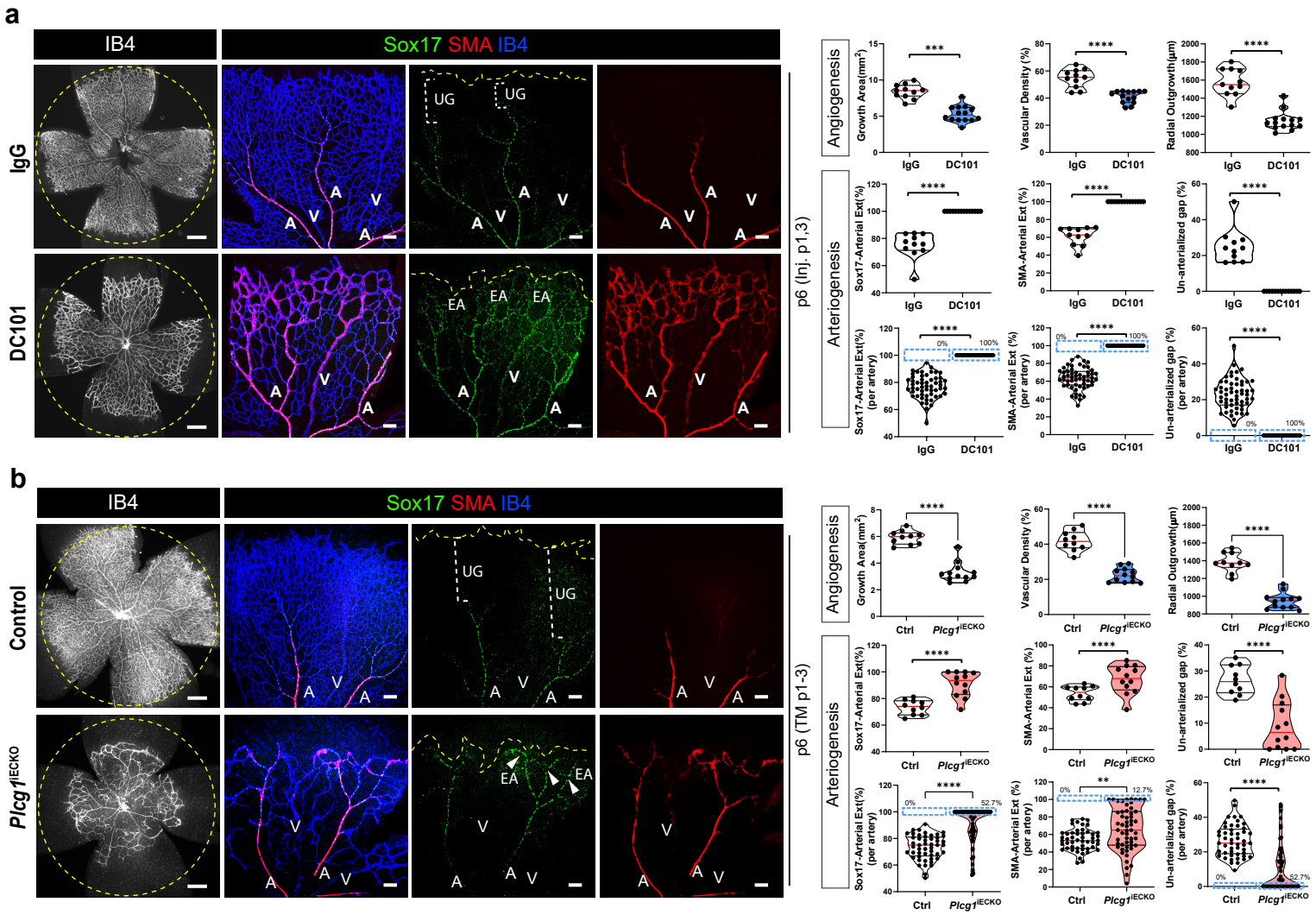

Fig.5 Fluid shear stress-induced arterial program is independent of VEGFR2 signaling.

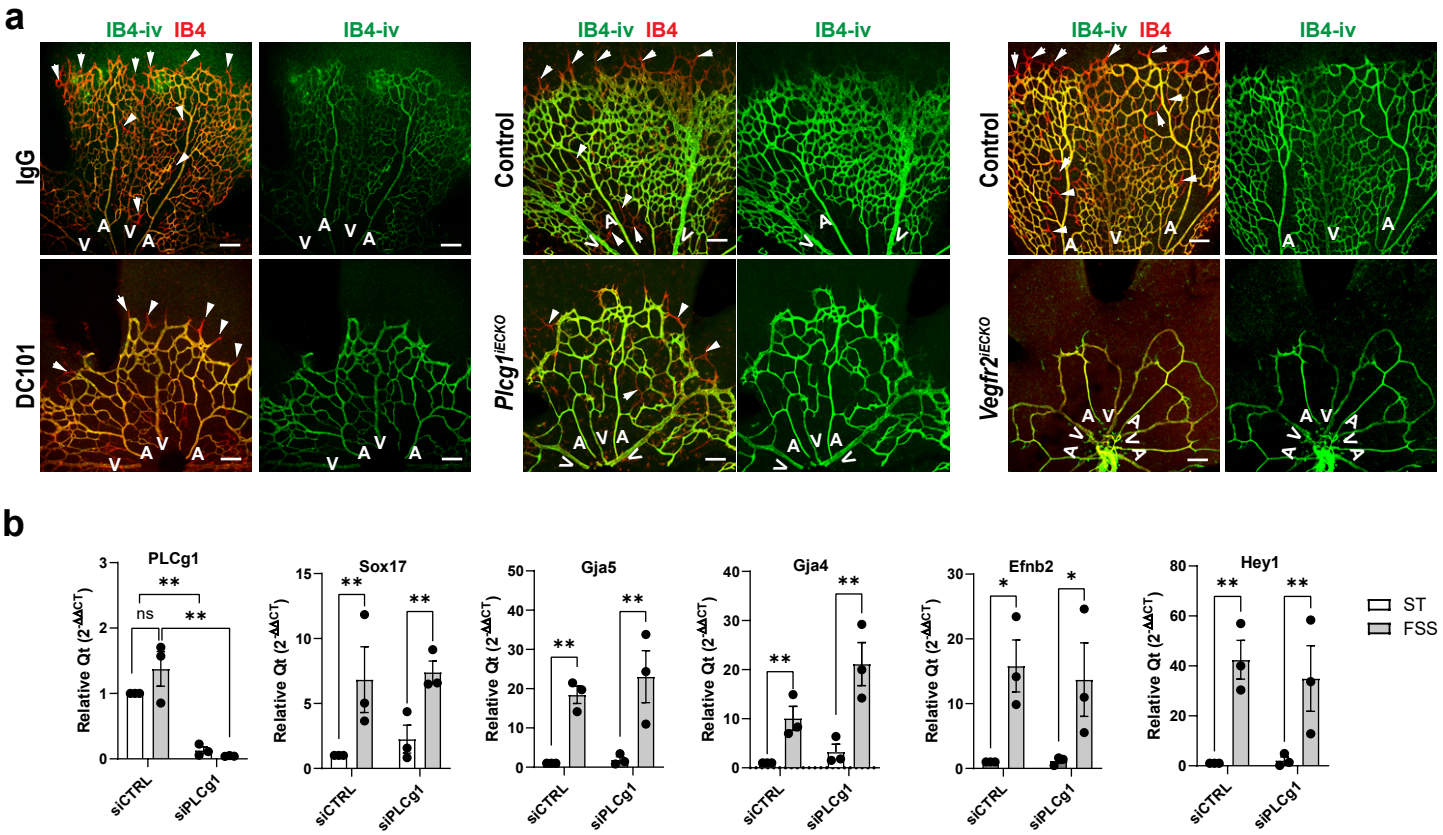

Fig.6 Blocking VEGFR2 signaling promotes capillary-to-artery transition in scRNAseq.

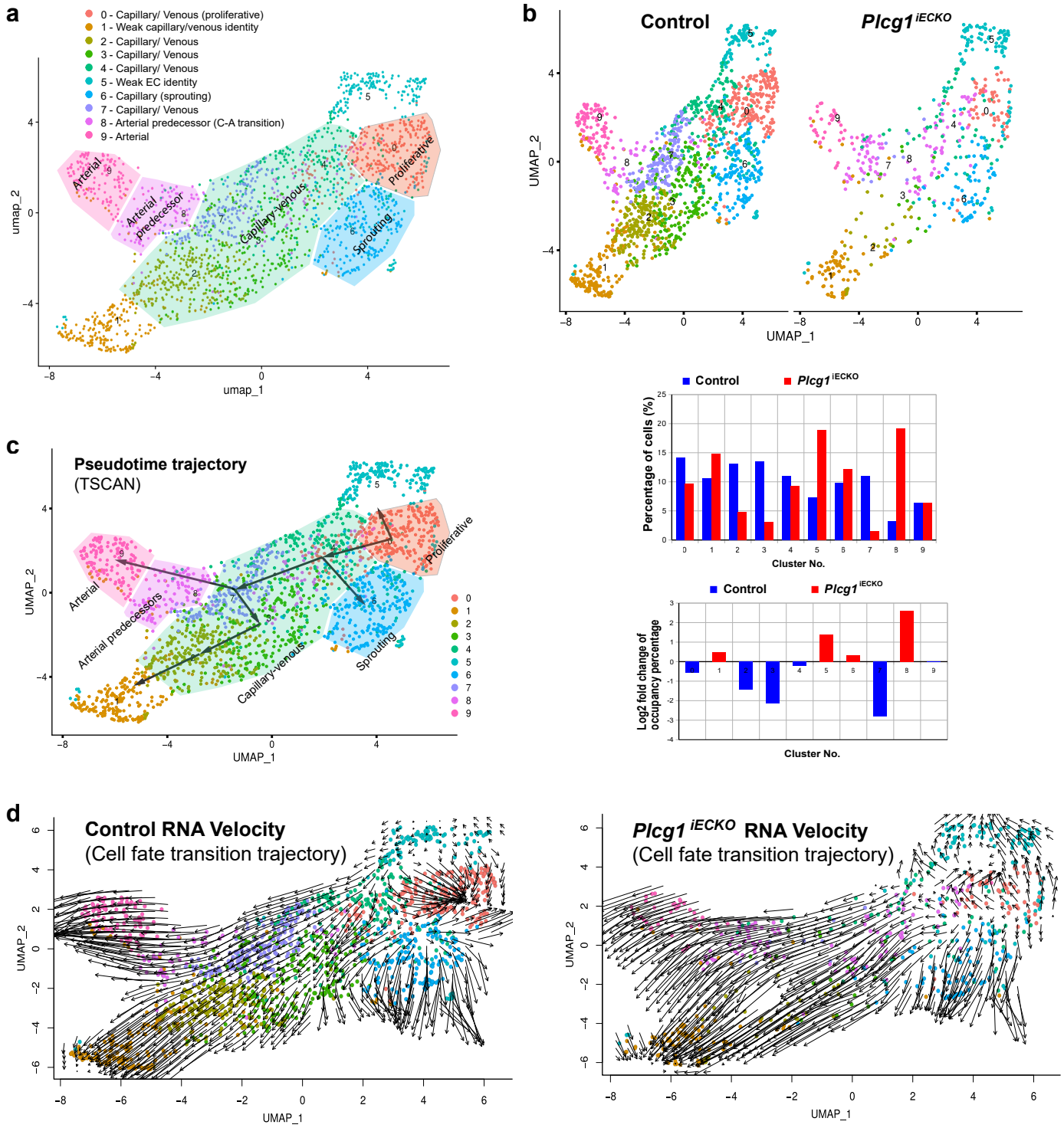

Fig.7 Sox17 is a mechanosensitive transcription factor essential for the FSS-induced arterial program.

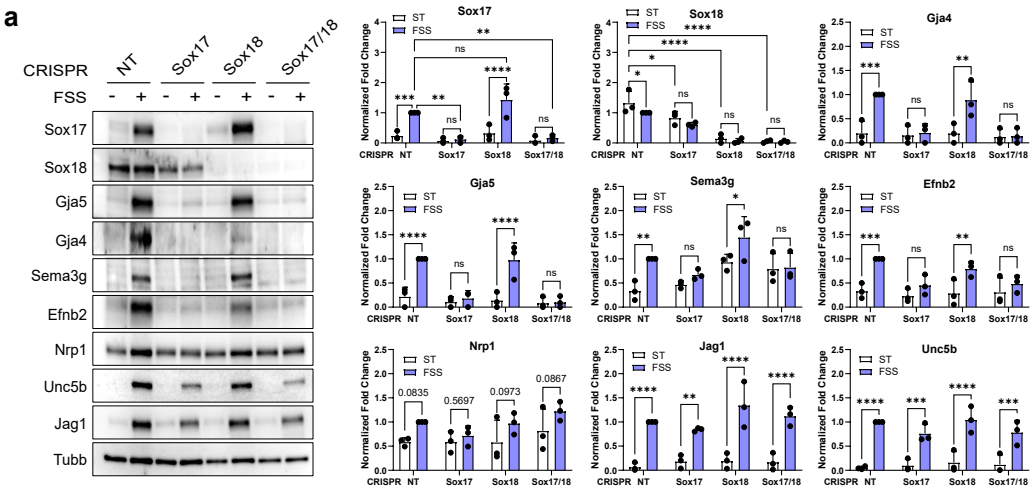

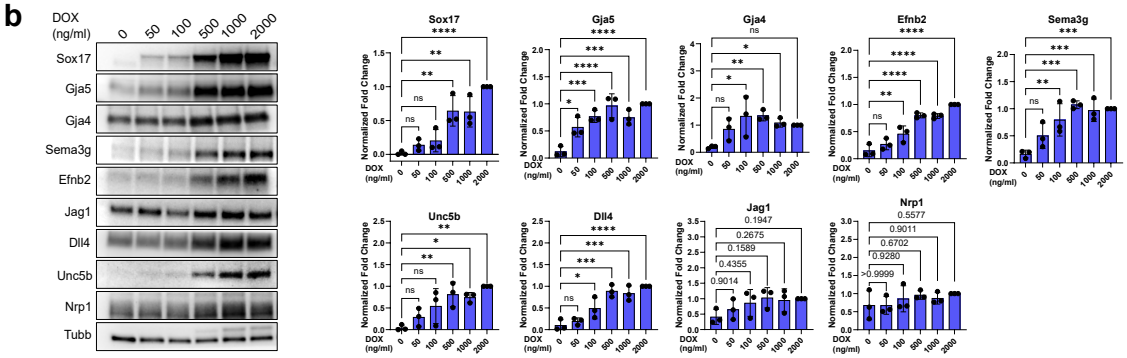

Fig. 8 VEGF antagonizes Sox17 transcription activity on arterial promoters and enhancers.

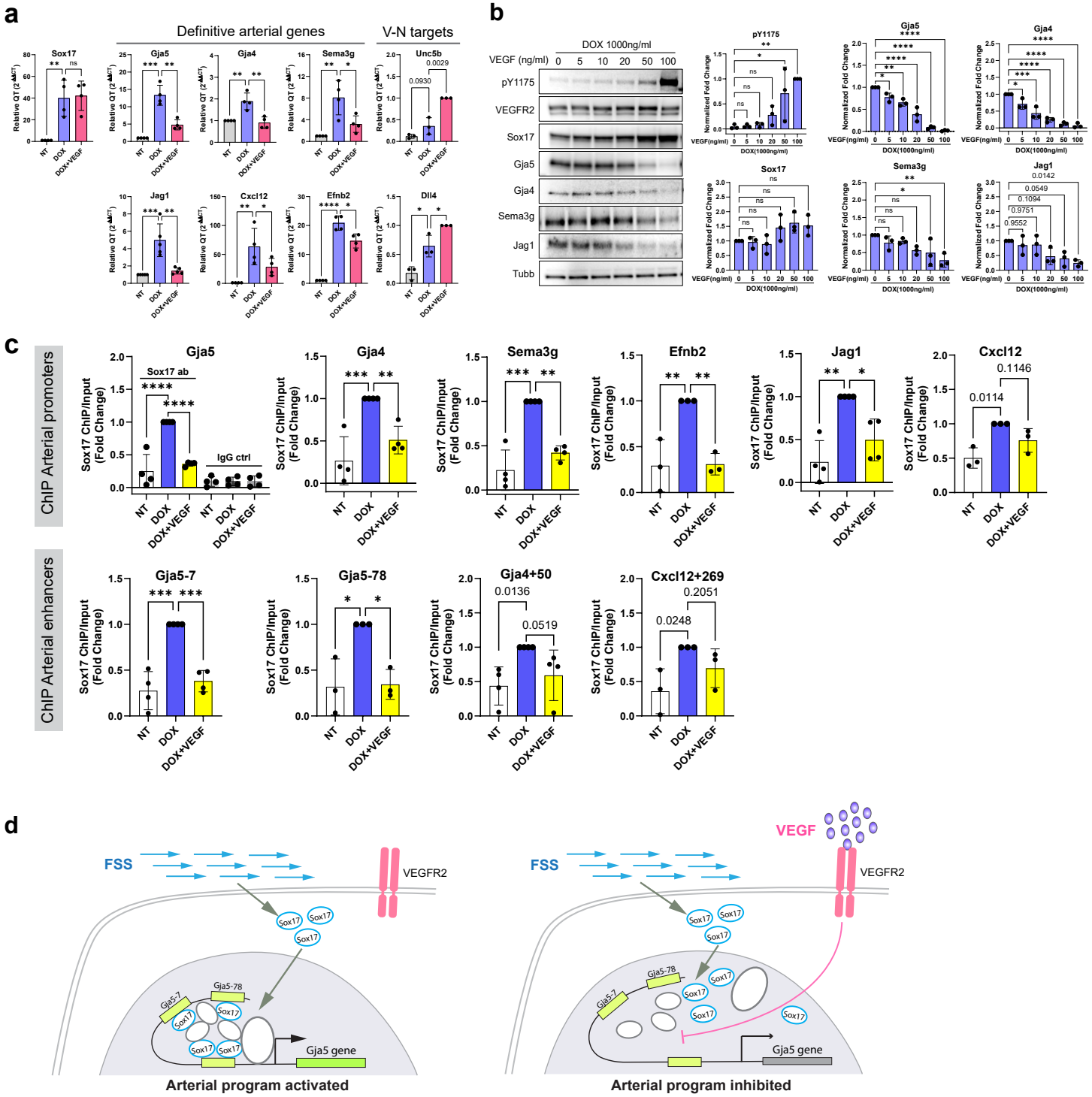
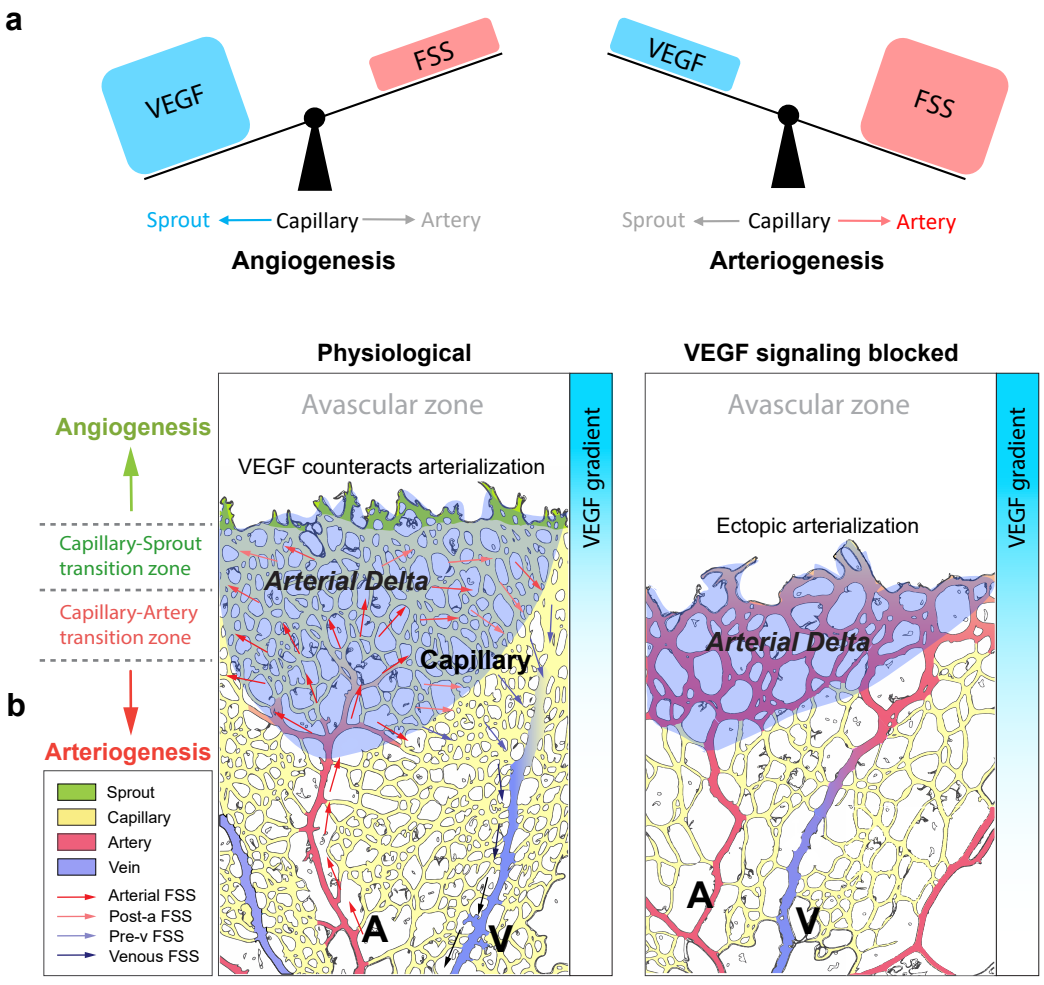
Fig.9 Angiogenic signaling is a physiological brake to counteract FSS-driven arteriogenesis.